University of Massachusetts Amherst
ScholarWorks@UMass Amherst

Masters Theses 1911 - February 2014

2011

Extensional-flow-induced Crystallization of Polypropylene

Erica E. Bischoff White
University of Massachusetts Amherst

Follow this and additional works at: https://scholarworks.umass.edu/theses

Part of the Mechanical Engineering Commons

Bischoff White, Erica E., "Extensional-flow-induced Crystallization of Polypropylene" (2011). *Masters Theses 1911 - February 2014*. 665.
Retrieved from https://scholarworks.umass.edu/theses/665

This thesis is brought to you for free and open access by ScholarWorks@UMass Amherst. It has been accepted for inclusion in Masters Theses 1911 - February 2014 by an authorized administrator of ScholarWorks@UMass Amherst. For more information, please contact scholarworks@library.umass.edu.

EXTENSIONAL-FLOW-INDUCED CRYSTALLIZATION OF POLYPROPYLENE

A Thesis Presented

By

ERICA E. BISCHOFF WHITE

Submitted to the Graduate School of the
University of Massachusetts Amherst in partial fulfillment
of the requirements for the degree of

MASTER OF SCIENCE IN MECHANICAL ENGINEERING

September 2011

Mechanical and Industrial Engineering

© Copyright by Erica E. Bischoff White 2011

All Rights Reserved

EXTENSIONAL-FLOW-INDUCED CRYSTALLIZATION OF POLYPROPYLENE

A Thesis Presented

By

ERICA E. BISCHOFF WHITE

Approved as to style and content by:

_____
Jonathan P. Rothstein, Chair

_____
H. Henning Winter, Member

_____
Robert W. Hyers, Member

_____
Donald L. Fisher, Department Head
Department of Mechanical and Industrial Engineering

DEDICATION

To my husband for your endless support, especially during the times of total discouragement. To my parents always encouraging me to explore and tinker when I was little. To Jack for reminding me when it was time to go to bed and to Dozer for giving me a great excuse to take a break and go for a walk.

ACKNOWLEDGMENTS

I would like to thank my advisor, Professor Jonathan Rothstein, for your nonpareil guidance; your post it notes are worth their weight in gold. I would also like to thank my committee members: Professor Henning Winter, thank you for being a kind source of advice and Professor Robert Hyers, thank you for your encouragement throughout the years and for helping me to get involved in research. Thank you to my lab mates for putting up with my whining and for helping me to tackle the oven. Thank you to Rick and Miles in the shop and especially to Robert for helping machine numerous rheometer plates and pieces for the oven. Thank you to Al for helping me with many wiring projects. I'd also like to Vikram Daga for helping me with the small-angle X-ray measurements. Lastly, I would like to thank NSF for making this project possible through funding.

ABSTRACT

EXTENSIONAL-FLOW-INDUCED CRYSTALLIZATION OF POLYPROPYLENE

SEPTEMBER 2011

ERICA E. BISCHOFF WHITE

B.S., UNIVERSITY OF MASSACHUSETTS AMHERST

M.S.M.E., UNIVERSITY OF MASSACHUSETTS AMHERST

Directed by: Professor Jonathan P. Rothstein

A filament stretching extensional rheometer with a custom-built oven was used to investigate the effect of uniaxial flow on the crystallization of polypropylene. Prior to stretching, samples were heated to a temperature well above the melt temperature to erase their thermal and mechanical histories and the Janeschitz-Kriegl protocol was applied. The samples were stretched at extension rates in the range of $0.01\text{s}^{-1} \le \dot{\varepsilon} \le 0.75\text{s}^{-1}$ to a final strain of $\varepsilon = 3.0$. After stretching, the samples were allowed to crystallize isothermally. Differential scanning calorimetry was applied to the crystallized samples to measure the degree of crystallinity. The results showed that a minimum extension rate is required for an increase in percent crystallization to occur and that there is an extension rate for percent crystallization is maximized. No increase in crystallization was observed for extension rates below a critical extension rate corresponding to a Weissenberg number of approximately $Wi = 1$. Below this Weissenberg number, the flow is not strong enough to align the tubes of constrained polymer chains within the melt and as a result there is no change in the final percent crystallization from the quiescent state. Beyond this critical extension rate, the percent crystallization was observed to increase to a

maximum, which was 18% greater than the quiescent case, before decaying again at higher extension rates. The increase in crystallinity is likely due to flow-induced orientation and alignment of tubes of constrained polymer chains in the flow direction. Polarized light microscopy verified an increase in number of spherulites and a decrease in spherulite size with increasing extension rate. In addition, small angle X-ray scattering showed a 7% decrease in inter-lamellar spacing at the transition to flow-induced increase in percent crystallization. Although an increase in strain resulted in a slight increase in percent crystallization, no significant trends were observed. Crystallization kinetics were examined as a function of extension rate by observing the time required for molten samples to crystallize under uniaxial flow. The crystallization time was defined as the time at which a sudden increase in the transient force measurement was observed. The crystallization time was found to decrease as one over the extension rate, even for extension rates where no increase in percent crystallization was observed. These results demonstrate that the speed of the crystallization kinetics is greatly enhanced by the application of extensional flow.

TABLE OF CONTENTS

Page

ACKNOWLEDGMENTS v

ABSTRACT vi

LIST OF TABLES x

LIST OF FIGURES xi

INTRODUCTION TO FLOW-INDUCED CRYSTALLIZATION OF POLYMERS 1

1.1 Introduction and Motivation 1

1.1.1 Extensional Flow-Induced Crystallization 4

EXPIRIMENTAL PROCEDURE 10

2.1 Experimental Outline 10

2.2 Materials and Sample Preparation 10

2.3 Extensional Rheology 11

2.3.1 Types of Extensional Rheology Experiments 13

2.3.2 Oven Fabrication 18

2.3.3 Sample Adhesion 19

2.4 Janeschitz-Kriegl Protocol 20

RESULTS AND DISCUSSIONS 22

3.1 Shear Rheometry 22

3.2 Extensional Rheometry 25

3.3 Crystallization Measurements 30

3.3.1 Differential Scanning Calorimetry 30

3.3.1.1 Peak Melting Temperature 33

3.3.1.2 Time-Temperature Transformation 34

3.3.2 Polarized-Light Microscopy 36

3.3.3 Small Angle X-ray Scattering 37

3.4 Extensional-Flow-Induced Crystallization with Varying Strain..... 40

3.5 Crystallization Time Measurements 41

3.6 Flow-Induced Crystallization of Branched Polypropylene..... 44

3.6.1 Materials 45

3.6.2 Shear Rheology 45

3.6.3 Extensional-Flow-Induced Crystallization Experiments 47

3.6.4 Results and Discussions 48

CONCLUSIONS..... 49

BIBLIOGRAPHY 52

LIST OF TABLES

Table Page

Table 3.1: Spectrum of modulus coefficients and relaxation times for linear polypropylene at T_c = 146°C. 24

Table 3.2: Spectrum of modulus coefficients and relaxation times for LCBPP at 150°C. 47

LIST OF FIGURES

Figure Page

Figure 1.1: Illustration of a shish-kebab crystal structure [Bassett (1981)]. 3

Figure 1.2: Electron spectroscopy image of shish-kebabs in polyethylene [Huong *et al.* (1992)]. 3

Figure 1.3: Pictorial representation of tubes of entangled polymer chains and extension of an individual chain within a tube [Schulz (2001)]. 6

Figure 1.4: Schematic of the TA Instruments extensional viscosity fixture [Hadinata *et al.* (2007)]. 6

Figure 2.1: Schematic diagram of a filament stretching rheometer with custom built oven. 12

Figure 2.2: Schematic of a fluid filament under extensional flow. 14

Figure 2.3: Diameter decay profiles for polypropylene at an extension rate of $\dot{\varepsilon} = 0.10s^{-1}$ at a temperature of T = 146°C using (○) type II and (△) type III experiments. The solid line represents the commanded diameter profile. 16

Figure 2.4: Transient force measurements for polypropylene at an extension rate of $\dot{\varepsilon} = 0.10s^{-1}$ at a temperature of T = 146°C using (○) type II and (▲) type III experiments. 16

Figure 2.5: Extensional viscosity measurements for polypropylene at an extension rate of $\dot{\varepsilon} = 0.10s^{-1}$ at a temperature of T = 146°C using (•) type II and (▲) type III experiments. 17

Figure 2.6: 3D models of rheometer plates (right) and sample (left) used for extensional rheology experiments. 19

Figure 3.1: The oscillatory shear master curves for polypropylene at T_c = 146°C. Included are the solutions of modulus master curves with storage modulus, G' (▼),and loss modulus, G''(•). 23

Figure 3.2: The oscillatory shear master curve with dynamic viscosity, η', for polypropylene at T_c = 146°C. 23

Figure 3.3: Filament stretching extensional rheology measurements of extensional viscosity as a function of accumulated Hencky strain for polypropylene melts stretched at various extension rates at T_c = 146°C.

Included are the solutions for extension rates of $\dot{\varepsilon} = 0.11\text{s}^{-1}$ (▷), $\dot{\varepsilon} = 0.15\text{s}^{-1}$ (○), and $\dot{\varepsilon} = 0.38\text{s}^{-1}$ (★). 26

Figure 3.4: Filament stretching extensional rheology measurements of extensional viscosity as a function of time for polypropylene melts stretched at various extension rates at T_c = 146°C. Included are the solutions for extension rates of $\dot{\varepsilon} = 0.11\text{s}^{-1}$ (▷), $\dot{\varepsilon} = 0.15\text{s}^{-1}$ (○), and $\dot{\varepsilon} = 0.38\text{s}^{-1}$ (★). The solid line represents the linear viscoelastic limit. 27

Figure 3.5: Filament stretching extensional rheology measurements of extensional viscosity as a function of extension rate for polypropylene melts stretched at T_c = 146°C to a fixed strain of $\varepsilon = 3.0$ 28

Figure 3.6: Filament stretching extensional rheology measurements of Trouton ratio as a function of Weissenberg number for polypropylene melts stretched at T_c = 146°C to a fixed strain of $\varepsilon = 3.0$ 29

Figure 3.7: DSC measurements showing with heat flow as a function of temperature. Included are polypropylene samples crystallized under quiescent conditions (□) and following a stretch with an extension rate of $\dot{\varepsilon} = 0.25s^{-1}$ at a fixed strain of $\varepsilon = 3.0$ (☆). 31

Figure 3.8: Percent crystallization as a function of extension rate and Weissenberg number for polypropylene samples crystallized following stretches to a fixed strain of $\varepsilon = 3.0$ 32

Figure 3.9: Peak melting temperature as a function of extension rate for polypropylene samples crystallized following stretches of various extension rates to a fixed strain of $\varepsilon = 3.0$ 33

Figure 3.10: DSC measurements showing heat flow as a function of time for polypropylene crystallizing isothermally at 145°C. 35

Figure 3.11: Time-temperature transformation diagram for polypropylene. Included are the results for the onset (■) and completion of crystallization (•). 35

Figure 3.12: Microscopy images taken through crossed polarizers of polypropylene samples showing the size of spherulites under a) quiescent conditions and following stretches with extension rates of b) $\dot{\varepsilon} = 0.10\text{s}^{-1}$ and c) $\dot{\varepsilon} = 0.25\text{s}^{-1}$ at a fixed strain of $\varepsilon = 3.0$. The direction of flow is aligned vertically. 36

Figure 3.13: Small angle X-ray scattering and two-dimensional scattering patterns [Wiesner (2008)]. 37

Figure 3.14: Two-dimensional small angle X-ray scattering patterns for polypropylene samples crystallized following stretches with extension rates of a) $\dot{\varepsilon} = 0.075\text{s}^{-1}$ and b) $\dot{\varepsilon} = 0.25\text{s}^{-1}$ to a final strain of $\varepsilon = 3.0$ and an extension rate of c) $\dot{\varepsilon} = 0.25\text{s}^{-1}$ to a final strain of $\varepsilon = 4.0$. The stretch direction is aligned horizontally to the scattering patterns. 39

Figure 3.15: Intensity of the scattering images presented in Figure 10 as a function of scattering vector, *q*, for polypropylene samples crystallized following stretches with extension rates of $\dot{\varepsilon} = 0.075\text{s}^{-1}$ (•) and $\dot{\varepsilon} = 0.25\text{s}^{-1}$ (△) to a final strain of $\varepsilon = 3.0$ and an extension rat of $\dot{\varepsilon} = 0.25\text{s}^{-1}$ (✯) to a final strain of $\varepsilon = 4.0$ 39

Figure 3.16: Percent crystallization as a function of final Hencky strain for polypropylene samples crystallized following stretches with extension rates of (▲) $\dot{\varepsilon} = 0.075\text{s}^{-1}$ and (■) $\dot{\varepsilon} = 0.25\text{s}^{-1}$ 41

Figure 3.17: Filament stretching extensional rheology measurements of force as a function of time for polypropylene samples crystallizing during extensional flows with extension rates of $\dot{\varepsilon} = 0.10\text{s}^{-1}$ (△) and $\dot{\varepsilon} = 0.15\text{s}^{-1}$ (•) at T_c = 146°C. 43

Figure 3.18: Crystallization time as a function of extension rate for polypropylene. 43

Figure 3.19: The oscillatory shear master curves for LCBPP at 150°C. Included are the solutions of modulus master curves with storage modulus, *G'* (▼), and loss modulus, *G"*(•)..... 46

Figure 3.20: The oscillatory shear master curve with dynamic viscosity, η', for LCBPP at 150°C. 46

CHAPTER 1

INTRODUCTION TO FLOW-INDUCED CRYSTALLIZATION OF POLYMERS

1.1 Introduction and Motivation

Manufacturing of plastics is carried out through the application of various processing techniques including extrusion, blow molding, injection molding, casting, fiber spinning, and rolling [Keller and Kolnaar (1997)]. All of these techniques rely on the application of heat and deformation of the material. The type and specifications of the process used to mold polymers has a significant impact on the properties of the final product. Many of these processes, such as blow molding and fiber spinning, primarily impose extensional flows on the polymer melt. Thus, understanding the rheological properties of and response of polymer melts in extensional flows is critical to a number of applications and industries.

The application of a sufficiently strong flow field to a polymer melt during processing will result in the alignment and in some cases the deformation of polymer chains. Flow is known to promote crystallization both by increasing the number of nucleation points for crystals to originate and by speeding up crystallization kinetics [Keller and Kolnaar (1997)]. Furthermore, when polymers are processed at high flow rates, crystal structures can form which bear superior physical properties [Van Puyvelde *et al.* (2008)]. A highly aligned, fairly continuous, crystal structure will result in a very stiff polymer [Mackley and Keller (1973)]. Extensional flows, by nature, are particularly effective at causing alignment and deformation of polymer chains in the flow direction [Sentmanat *et al.* (2010)].

Flow is known to facilitate the crystallization of polymers through alignment and deformation of entangled tubes of constrained polymer chains. The stretching and aligning of polymer chains by the flow reduces the entropy of the system as well as the change in free energy required for crystallization to take place [Mackley and Keller (1975)]. The reduction in entropy results in an increase in the melting temperature of the polymer and effectively increases the degree of supercooling, thereby aiding the crystallization process. The extension of polymer chains also reduces the kinetic barrier which must be overcome for crystallization to occur because the state of the polymer chain in the melt is closer to that of the final crystal when it is extended as compared to when it is a random coil [Keller and Kolnaar (1997)].

In addition to changing the final crystallinity and form of the final crystal state, the application of flow is known to have a large impact on the crystallization kinetics of polymers. For fairly quickly crystallizing polymers, such as polypropylene, an increase in supercooling alone (under quiescent conditions without the additional kinetic assistance provided by flow) can result in a significant increase in the number of nucleation points [Janeschitz-Kriegl *et al.* (1995)]. The introduction of flow while in the supercooled state can have an even greater impact [Janeschitz-Kriegl (2003)], reducing the time required to fully crystallize to by orders of magnitude [Haas and Maxwell (1969)].

When segments of constrained polymer chains are aligned and stretched in the flow direction, the polymer can form a shish-kebab crystal structure [Pennings *et al.* (1983)]. In shish-kebabs, lamellar crystals grow outward from an aligned cylindrical core. An illustration of a shish-kebab crystal structure is shown in Figure 1.1. In Figure 1.2, shish-kebabs in polyethylene can be seen to be aligned diagonally in an electron

spectroscopy image. In order for shish-kebabs to nucleate, sufficient chain extension and orientation is required [Mackley (1975)]. Therefore, an elongational component must exist in the flow for a shish-kebab structure to evolve, whether it be in a purely extensional flow or a shear flow with a tangential velocity gradient that results in local chain extension [Mackley *et al.* (1975)]. However, because shear flows result in a rotation of the tubes of polymer chains away from the direction of extension they are less effective at producing orientation than extensional flows [McKinley and Sridhar (2002a)]. In addition, deformation in the flow direction caused by extensional flow enhances the thread-like precursors which are required for the formation of shish-kebabs [Chellamuthu *et al.* (In Press 2011)].

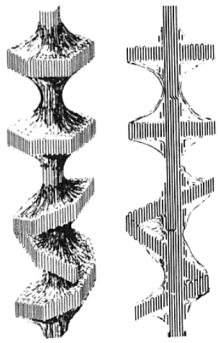

Figure 1.1: Illustration of a shish-kebab crystal structure [Bassett (1981)].

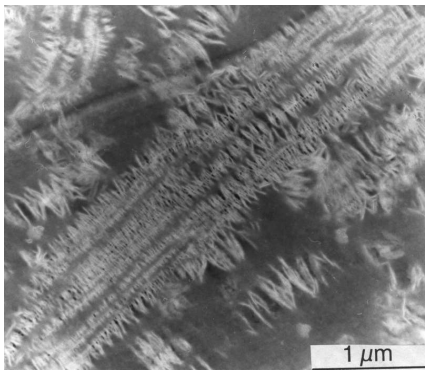

Figure 1.2: Electron spectroscopy image of shish-kebabs in polyethylene [Huong *et al.* (1992)].

A large amount of research has been dedicated to studying the effect of shear flows on the crystallization kinetics and morphologies of polymers. Studies by Kumaraswamy *et al.* [Kumaraswamy *et al.* (1999)] and Hass *et al.* [Haas and Maxwell (1969)] have demonstrated that, under strong shear flow, crystallization kinetics become faster at high temperatures close to the melt temperature. This effect can be attributed to the facilitation of flow-induced alignment caused by the increased mobility of constrained tubes of polymer chains at high temperatures [Kumaraswamy *et al.* (1999)].

Elmoumni *et al*. [Elmoumni and Winter (2006)] determined the effect of varying strain on the crystal structure of various molecular weight polypropylene samples by pre-shearing them at a constant Weissenberg number of $Wi = 1$. The Weissenberg number, $Wi = \lambda\dot{\varepsilon}$, is a measure of the strength of the flow and is defined by the ratio of the characteristic relaxation time of the fluid, λ, to the characteristic timescale of the flow, $1/\dot{\varepsilon}$, where $\dot{\varepsilon}$ is the applied strain rate. Elmoumni *et al*. [Elmoumni and Winter (2006)] performed in-situ polarized light microscopy along with wide-angle X-ray diffraction on the crystallized samples and were able to determine that an accumulated shear strain of $\gamma = 600$ was required for the transition from a spherulitic to shish-kebab crystal structure to occur. Van Puyvelde *et al.* [Van Puyvelde *et al.* (2008)] used a shear cell to apply a strong shear flow to poly-1-butene and demonstrated that both a critical shear strain and critical shear rate were required to obtain a shish-kebab crystal structure and that the critical shear strain decreased with increasing shear rate.

1.1.1 Extensional Flow-Induced Crystallization

It is important to investigate the effects of extensional flow on crystallization of polymers in addition to shear flow since, as discussed previously, so many manufacturing

processes are, to some extent, include extensional flow components. Furthermore, the strain requirement for flow-induced crystallization is less in extension than in shear [Sentmanat *et al.* (2010)]. Even though extensional flows are able to generate greater molecular alignment than shear flows [Hadinata *et al.* (2007)] and therefore more effectively enhance the resulting crystallization kinetics and morphological changes, very few studies have systematically investigated the effect of pure extensional flows on crystallization [Chellamuthu *et al.* (In Press 2011); Hadinata *et al.* (2007); Sentmanat *et al.* (2010)].

Extensional flow can have a varying effect on the microstructure of a polymer, which is highly dependent on the strength of the flow. The Weissenberg number is used to characterize the strength of the flow. In order to calculate the Weissenberg number, the characteristic relaxation time of the fluid must first be determined. There are many relaxation times for entangled polymer systems; the ones of most interest for this study are the disengagement time, λ_d, and Rouse time, λ_R. The disengagement time is a measure of the time it takes for the tubes of polymer chains to become re-entangled after being separated by flow. This relaxation time is used to calculate the Weissenberg number. The Rouse time, which is much shorter than the disengagement time, is the relaxation time for a polymer chain within a tube. The Rouse time is a function of the average number of entanglements per chain of polymer, $Z = M_w / M_e$, and is calculated by $\lambda_R = \lambda_d / 3Z$ [Rothstein and McKinley (2002a)]. An illustration of the extension of a polymer chain within an entangled tube is shown in Figure 1.3. At low Weissenberg numbers, the flow is not strong enough to have any lasting effect and the polymer chains have time to relax. At $Wi \geq 1/2$, the flow becomes strong enough to align the entangled

tubes and it is not until $Wi > \lambda_d / \lambda_{Rouse}$, or $Wi > 3M_w / M_e$, that the polymer chains within the tubes are extended [Rothstein and McKinley (2002a)].

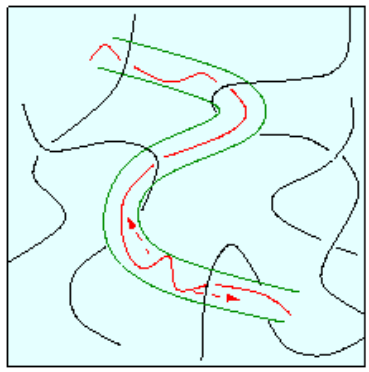

Figure 1.3: Pictorial representation of tubes of entangled polymer chains and extension of an individual chain within a tube [Schulz (2001)].

Extensional-flow-induced crystallization was studied and compared to shear-flow-induced crystallization of a high molecular weight isotactic poly-1-butene by Hadinata *et al.* [Hadinata *et al.* (2007)]. They used a TA Instruments extensional viscosity fixture (EVF) on a rotational rheometer to apply an extensional flow to the melts. A schematic of the EVF can be seen in Figure 1.4.

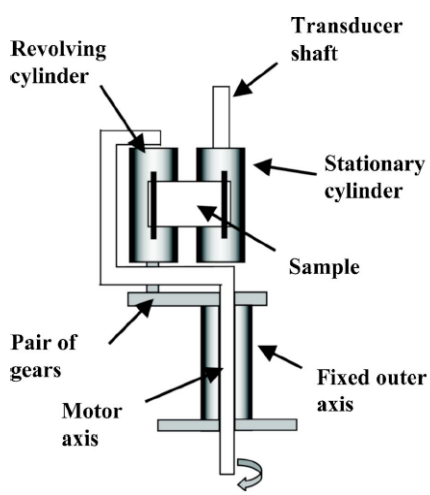

Figure 1.4: Schematic of the TA Instruments extensional viscosity fixture [Hadinata *et al.* (2007)].

It is important to note that strain which can be applied using an extensional viscosity fixture is limited by a full rotation of the drums, after which point the fluid begins to wrap on itself. In the case of the TA Instruments EVF, the maximum strain that can be applied is $\varepsilon = 4.9$. By marking the onset of crystallization to be the time at which a sudden increase in extensional viscosity was observed, Hadinata *et al.* [Hadinata *et al.* (2007)] were able to deduce that flow-induced crystallization occurred in extension at one hundredth of the time it took to occur under shear. They were also able to show that, beyond a critical extension rate, the onset of crystallization time decreased roughly with the inverse of the extension rate. They attributed this result to the extensional flows ability to orient polymer chains. At low extension rates, the flow was too slow to compete with the relaxation of the polymer and no change in crystallization onset time was observed. Their results demonstrate that extensional flow is a stronger agent for nucleating crystals than shear flow. In addition, they found that the onset of crystallization time, for extension rates of $\dot{\varepsilon} \geq 0.01\text{s}^{-1}$, did not vary with temperature. These results indicate that, kinetically, the crystallization kinetics were dominated by the applied flow field and not the underlying thermal motion of the polymer chains. Unfortunately, in their experiments they were unable to measure either the final percent crystallization or the final crystal structure due to sagging of the samples within their extensional rheometer. [Hadinata *et al.* (2007)]

More recently, Sentmanat *et al.* [Sentmanat *et al.* (2010)] used a Sentmanat extensional viscosity fixture on rotational rheometer (SER extensional rheometer) to apply uniaxial extensional flow to an ethylene-based butane plastomer. This device is similar to the EVF used by Hadinata *et al.* [Hadinata *et al.* (2007)]. Sentmanat *et al.*

[Sentmanat *et al.* (2010)] mitigated the problem of sample sagging in the rheometer by quenching the samples after stretching with water. The results of their experiments showed that a higher degree of crystallization could be achieved by stretching samples at a temperature near the peak melting temperature. These results were also explained by increased mobility of polymer chains at high temperatures. [Sentmanat *et al.* (2010)]

One of the difficulties of studying extensional-flow-induced crystallization falls in the design of an experiment which includes a well-defined extensional flow and well-defined temperature protocol [Hadinata *et al.* (2007)]. Due to sample sagging, SER and EVF extensional rheometers are not suitable for studies that require the preservation of samples for crystallization analysis. Although the samples can be quenched with water to solidify them before sagging occurs, a more ideal temperature protocol is necessary for reliable crystallization measurements.

Recently, Chellamuthu *et al.* [Chellamuthu *et al.* (In Press 2011)] were able to perform extensional-flow-induced crystallization measurements of isotactic poly-1-butene using the same filament stretching rheometer and oven described in this paper. Even though their samples did not display significant strain hardening or extensional thickening, they found that the application of extensional flow had significant effects on crystallization of the polymer. Using a differential scanning calorimeter, they measured that the degree of crystallinity increased from 45% to 62% with an increase in extension rate from $\dot{\varepsilon} = 0.01\text{s}^{-1}$ to $\dot{\varepsilon} = 0.50\text{s}^{-1}$ for a fixed imposed strain. They also found that there was a critical extension rate below which no flow-induced crystallization occurred. More interestingly, they found that there exists an extension rate for which the percent crystallization was maximized. Above this maximum, the percent crystallization

decreased to a value which was still greater than the percent crystallization obtained for the quiescent case. One of the objectives of this study is to determine if this trend is specific to poly-1-butene or if it is robust and exists in other polymers as well. [Chellamuthu *et al.* (In Press 2011)]

In addition to differential scanning calorimetry measurements, Chellamuthu, *et al.* [Chellamuthu *et al.* (In Press 2011)] also performed small angle X-ray scattering of the crystallized samples. The results showed the presence of a highly oriented crystal structure in samples which had experienced high extension rates, demonstrating the development of a shish-kebab morphology as a result of molecular alignment caused by the application of strong extensional flow. They attributed the observed increase in percent crystallization to the increase in deformation caused by the flow and resulting in the strengthening of the thread-like precursors which lead to the growth of a shish-kebab crystal structure. The results of these experiments demonstrate the ability of extensional flows to align tubes of constrained polymer chains, develop the thread-like precursors required for the growth of shish-kebabs, and increase nucleation points. Whether or not a shish-kebab structure ensues for polypropylene as a result of the application of extensional flow will also be a focus of this study. [Chellamuthu *et al.* (In Press 2011)]

The investigation of flow-induced crystallization of polypropylene by use of a filament stretching rheometer is the focus of this research. In the following sections of this paper, the experimental processes for characterizing changes in percent crystallization through the use of filament stretching extensional rheology methods are described. This thesis concludes with a discussion about the results of the experiments.

CHAPTER 2

EXPIRIMENTAL PROCEDURE

2.1 Experimental Outline

Polypropylene samples were prepared for shear and extensional rheology experiments. Oscillatory shear rheology measurements were performed to measure the polymers viscoelastic response and determine its characteristic relaxation time. Extensional rheology experiments were performed over a range of extension rates at a single strain and the Janeschitz-Kriegl protocol was applied. Extensional viscosity measurements were taken to probe the polymers response extensional flow of varying strength. After stretching, the samples were crystallized isothermally and measurements were taken to determine the final percent crystallization and crystal structure.

2.2 Materials and Sample Preparation

Extensional-flow-induced crystallization was studied for a commercial grade HB205TF, polypropylene, melt. The material was provided by Borealis in the form of pellets and was free of added nucleating agents. HB205TF has a molecular weight of $M_w = 600,000\text{g/mol}$ and a polydispersity of 4.2. The entanglement molecular weight is on the order of $M_e = 7,000\text{g/mol}$. The method for calculating the molecular weight of entanglements is described in Section 3.1.

Before being tested in the shear and extensional rheometers, the pellets were first molded to fit the plate geometry. The pellets were melted in a custom-built hot press under vacuum at 200°C and pressed into a mold. The mold was allowed to cool, after

which additional pellets were added, and the process was repeated until the samples were free of voids.

2.3 Extensional Rheology

A filament stretching extensional rheometer (FiSER) was used to apply a homogeneous uniaxial extensional flow to the melts. Transient force and midpoint radius were measured simultaneously as the fluid filament, placed between its two end plates, was stretched. A schematic of the filament stretching rheometer and oven is shown in Figure 2.1. A complete description of the design and operating space of the filament stretching rheometer used in these experiments can be found in the literature [Chellamuthu *et al.* (In Press 2011); Rothstein (2003); Rothstein and McKinley (2002a); Rothstein and McKinley (2002b)] and a more detailed history of the technique can be found in the following papers by the McKinley and Sridhar groups [Anna *et al.* (2001); McKinley and Sridhar (2002b); Tirtaatmadja and Sridhar (1993)].

The goal of extensional rheometry is to produce a motion between the two endplates such that the resulting extension rate, imposed on the fluid filament, is constant; this is often difficult to accomplish. The extension rate is calculated by,

$$\dot{\varepsilon} = -\frac{2}{R_{mid}(t)}\frac{dR_{mid}(t)}{dt}, \tag{2.1}$$

where $R_{mid}(t)$ is the radius at the midpoint of the filament. The deformation imposed upon the fluid filament can be described in terms of a Hencky strain,

$$\varepsilon = -2\ln\left(R_{mid}/R_0\right), \tag{2.2}$$

where R_0 is the initial midpoint radius of the fluid filament. The strength of the extensional flow, as stated previously, is characterized by the Weissenberg number. The

elastic tensile stress difference generated within the fluid filament can be calculated from the algebraic sum of the total force measured by the load cell, F_z, if the weight of the fluid and the surface tension are taken into account and inertial effects are ignored [Anna *et al.* (2001)];

$$\langle \tau_{zz} - \tau_{rr} \rangle = \frac{F_Z}{\pi R_{mid}^2} + \frac{1}{2}\frac{\rho g(\pi L_0 R_0^2)}{\pi R_{mid}^2} - \frac{\sigma}{R_{mid}} \tag{2.3}$$

where L_0 is the initial endplate separation, σ is the equilibrium surface tension of the fluid, and ρ is the density of the fluid.

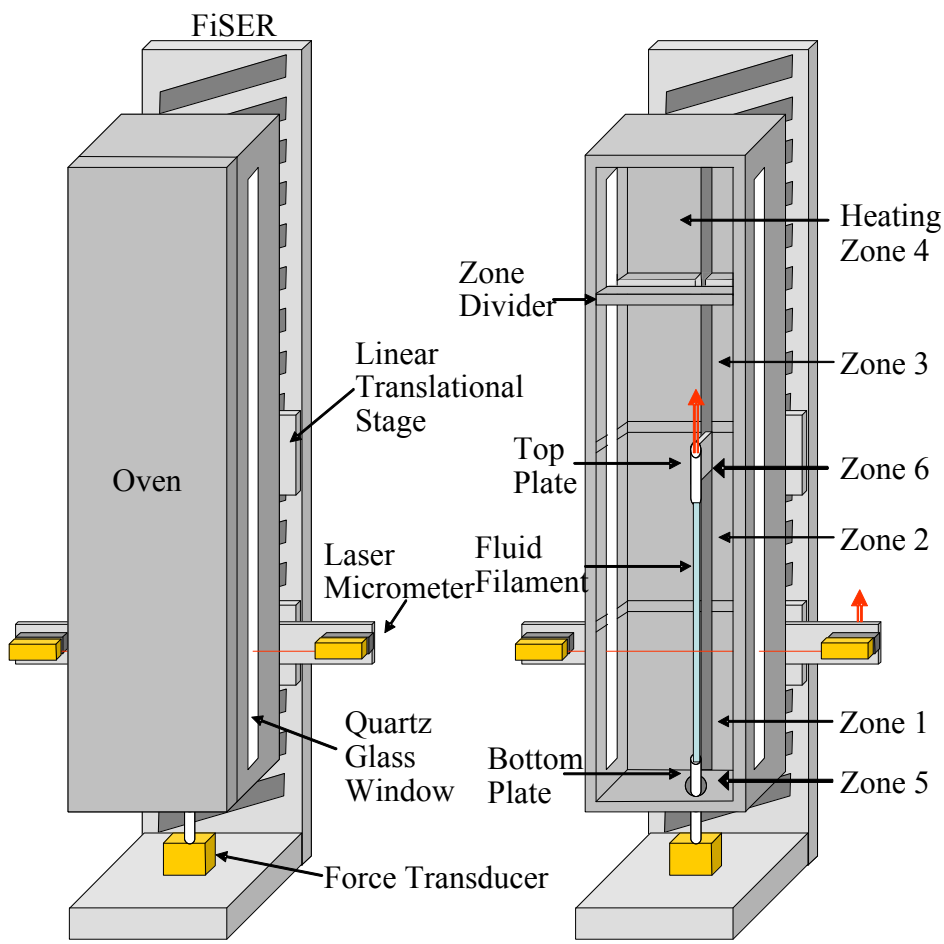

Figure 2.1: Schematic diagram of a filament stretching rheometer with custom built oven.

The extensional viscosity may be extracted from the principal elastic tensile stress by dividing by the extension rate, $\eta_E = \langle \tau_{zz} - \tau_{rr} \rangle / \dot{\varepsilon}$, and is often non-dimensionalized as a Trouton ratio,

$$Tr = \eta_E(\dot{\varepsilon}) / \eta(\dot{\varepsilon}\sqrt{3}) \tag{2.4}$$

where η_E is the transient extensional viscosity as a function of extension rate and η is the shear rate dependant viscosity of the fluid, which is taken at a shear rate that has been translated to the corresponding extension rate. For a Newtonian fluid, the Trouton ratio is constant $Tr = 3$, while a non-Newtonian fluid can strain harden such that very large Trouton ratios can be achieved under flows of Weissenberg numbers greater than $Wi > ½$ [McKinley and Sridhar (2002b)].

2.3.1 Types of Extensional Rheology Experiments

The ideal extensional rheometry experiment, as fore mentioned, is one in which the endplates are driven apart such that the fluid filament experiences a constant extension rate, i.e. an exponential diameter decay with time. This can be challenging due to the nature of extensional flows and the presence of additional driving forces such as surface tension. In addition, the extension rate is not constant over the entire fluid filament due to the attachment at the endplates, as shown in Figure 2.2. As a result of the no-slip boundary condition at the endplates, a shear flow develops near the endplates [Anna *et al.* (1999)]. If the extension rate at the mid-point of the fluid filament is controlled such that it acts as a cylinder under uniaxial extension, then the midsection of the fluid filament will behave as if it is under an ideal extensional flow and shear effects at the ends can be neglected [Anna *et al.* (1999)]. There are three types of filament

stretching experiments which can be carried out using the filament stretching rheometer. These experiments have been and coined type I, type II, and type III experiments by Kolte *et al.* [Kolte *et al.* (1997)]. During type I experiments, the endplates are driven apart with an exponential velocity profile,

$$L(t) = L_0 e^{\dot{\varepsilon} t}, \tag{2.5}$$

and the extension rate, $\dot{\varepsilon}$, is assumed to be constant.

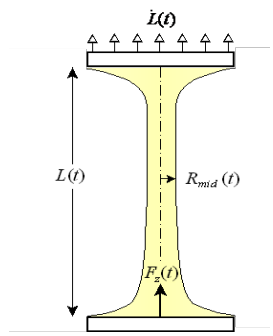

Figure 2.2: Schematic of a fluid filament under extensional flow.

The force evolution is measured as the fluid filament is stretched and the resulting Hencky strain, stress, and viscosity are calculated. Since, the extension rate is assumed to be constant, the Hencky strain can be calculated as $\varepsilon = \dot{\varepsilon} t$. Type II experiments take the same approach to driving the flow but, the extension rate is not assumed to be constant. Rather, it is calculated from diameter measurements taken at the midpoint of the fluid filament. The extension rate and Hencky strain are calculated as defined in Equations 2.1 and 2.2, respectively. Although type II experiments account for varying extension rates, the imposed flow field is still not ideal.

In type III experiments, a constant extension rate is achieved by requiring the endplates to be driven in manner which forces the diameter decay of the fluid filament to be exponential. Thus, the extension rate is constant and the Hencky strain is simplified

from Equation 2.2 to $\varepsilon = \dot{\varepsilon} t$. Type III experiments are difficult to carry out because they require one of two techniques, the use of a control system capable of quickly measuring and responding to changes in diameter or an iterative process [Kolte *et al.* (1997)]. The iterative techniques begins with performing a type II experiment and then using the diameter measurements to determine the velocity profile of the endplates which results in an exponential diameter decay [Anna *et al.* (1999)]. The results of the iterative technique are not necessarily independent of extension rate or the fluid used, for that reason a closed-loop control system was designed and implemented for the experiments in this study.

A proportional-integral-derivative (PID) control system was designed using LabView to control the extension rate of a fluid filament in the filament stretching rheometer. The PID controller simultaneously takes measurements of diameter and commands the velocity of the endplates. The measured diameter at a given instant in time is used to estimate the required velocity at the next time step. The PID controller is able to sample the diameter at a rate of 6Hz. Transient diameter measurements are shown with the commanded diameter profile in Figure 2.3 for type II and type III experiments performed in the filament stretching rheometer on polypropylene samples at an extension rate of $\dot{\varepsilon} = 0.10s$. Note that a constant extension rate corresponds to a linear diameter decay on a log plot. Type III experiments were found to be much more adept at maintaining a constant extension rate throughout the entire stretch where as type II experiments are only able to achieve a constant extension rates for small strains. The only disadvantage of closed-loop control of diameter is that the control system often results in abrupt changes in the velocity profile of the endplates which can cause undesirable

fluctuations in force. For this reason, real-time control systems have been found, in the past, to be inferior to iterative techniques [Anna *et al.* (1999)].

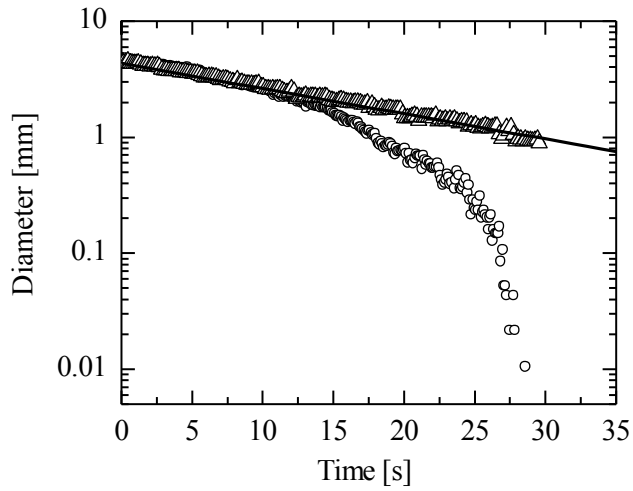

Figure 2.3: Diameter decay profiles for polypropylene at an extension rate of $\dot{\varepsilon} = 0.10s^{-1}$ at a temperature of T = 146°C using (○) type II and (△) type III experiments. The solid line represents the commanded diameter profile.

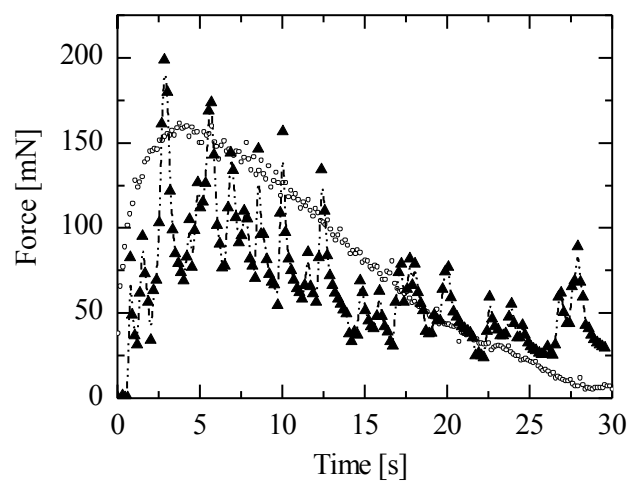

Figure 2.4: Transient force measurements for polypropylene at an extension rate of $\dot{\varepsilon} = 0.10s^{-1}$ at a temperature of T = 146°C using (○) type II and (▲) type III experiments.

In the experiments performed in this study, fluctuations in force were apparent (refer to Figure 2.4), they did not, however impair the measurements of extensional viscosity. Both type II and type III experiments were found to result in a similar trend in

extensional viscosity, as demonstrated in Figure 2.5. Note that for type II experiments, extensional viscosity is plotted as a function of the commanded extension rate in Figure 2.5. Therefore the variance in extensional viscosity between type II and type III experiments is likely due to the uncertainty in the extension rate of type II experiments.

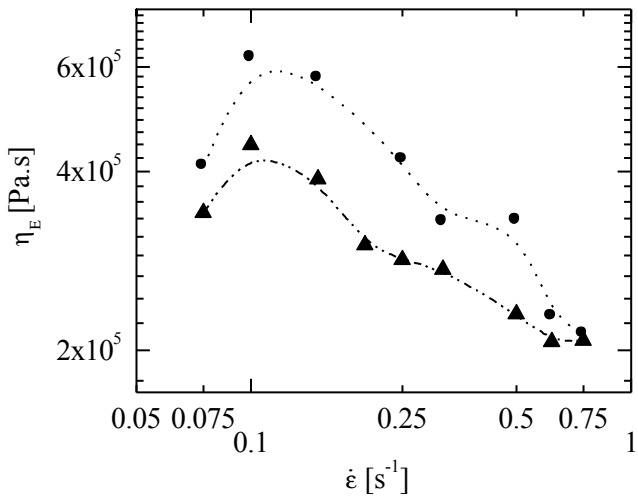

Figure 2.5: Extensional viscosity measurements for polypropylene at an extension rate of $\dot{\varepsilon} = 0.10s^{-1}$ at a temperature of T = 146°C using (•) type II and (▲) type III experiments.

Currently, the PID control system is able to control the diameter of a fluid filament within 10% of the required diameter for extension rates up to $\dot{\varepsilon} = 1.0\text{s}^{-1}$ and down to diameters of approximately $D = 100\mu\text{m}$. Diameters below $D = 100\mu\text{m}$ can not be clearly resolved with the laser micrometer. Extension rates above $\dot{\varepsilon} = 1.0\text{s}^{-1}$ were observed to result in a diameter decay which deviates from the exponential profile. The system's ability to control at higher extension rates was found to be limited by the sampling rate of the controller. A faster sampling ability would facilitate control at higher extension rates. All things considered, this PID control system is a proficient approach to driving extensional flows in a filament stretching rheometer.

2.3.2 Oven Fabrication

In order to apply filament stretching techniques to polymer melts, an oven was designed and integrated with the filament stretching rheometer. A schematic of the filament stretching rheometer and oven is shown in Figure 2.1. The oven is a 2m tall, ¼ in. thick, aluminum shell which is insulated interiorly with ceramic fibre. The insulation is lined with aluminum sheets to prevent dust from contaminating samples in the rheometer. The oven is designed such that the fluid filament is fully enclosed as it is stretched. Care was taken in placement of the heating elements to ensure uniform heating of the sample before and during stretching.

The oven consists of six independently controlled heating zones, four of which are separated by horizontal plates that serve to reduce natural convection. All four zones are shown in Figure 2.1 however, for clarity only a single divider is shown. For temperature measurements, thermocouples were installed in all six heating zones. Temperature of the fluid filament is controlled locally with two heating zones. One zone consists of a band heater surrounding the bottom plate. The other consists of a cartridge heater built into the top plate; allowing the heater to translate with the motion of the top plate. The placement of these two zones ensures both heaters remain in close proximity to the fluid filament during the entire process. The thermocouples of these two zones are placed such that they are approximately 1mm from the top and bottom of the sample. The upper thermocouple is attached to the top plate so that it also follows the sample during stretching. Temperature is able to be controlled to an accuracy of ±1˚C via a PID temperature control system (Omega Temperature Controller model CN616TC1).

2.3.3 Sample Adhesion

Polypropylene displays weak adhesive properties due to its low surface energy. Adhesion can be achieved by chemically altering the polymer, i.e. blending or grafting; however grafting can lead to branching, cross-linking, and degradation of the material [Shreya (2008)]. Blending has been found to be effective at increasing the adhesion of polypropylene to metallic surfaces [Belyi (1971); Shreya (2008)]. Blending was not an option, as introducing additional materials into the polypropylene samples would further complicate the results of the study. Often, increasing the surface area to which the sample is adhered can help increase adhesion. Cross-hatched plates were found to be effective, but could only maintain adhesion of the samples at low extension rates. The ultimate objective was to create plates that could anchor a polymer-melt filament at any extension rate. Ergo, a final set of plates was designed to rely on geometric constraints rather than adhesion properties of the polymer. These plates effectively grasp and pull dumbbell shaped samples, refer to Figure 2.6. This design was found to be highly functional at all extension rates tested.

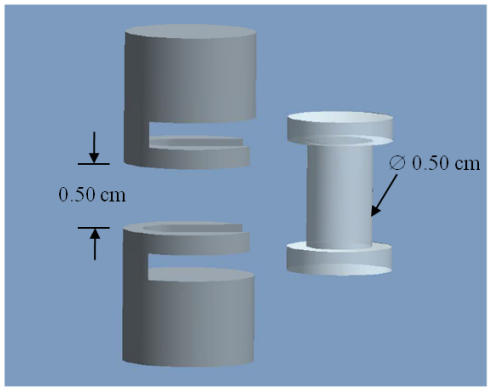

Figure 2.6: 3D models of rheometer plates (right) and sample (left) used for extensional rheology experiments.

2.4 Janeschitz-Kriegl Protocol

The Janeschitz-Kriegl protocol was implemented to study flow-induced crystallization of polypropylene. The Janeschitz-Kriegl protocol, often referred to as short-term shearing, began as a way to study flow-induced crystallization under shear flow. In order to achieve crystallization at high temperatures, near or above the melting temperature, a great amount of shearing is often necessary. The short-term shearing protocol allows flow-induced crystallization to be studied at lower temperatures, at which the samples are slightly super-cooled, by applying flow for a short period of time [Liedauer *et al.* (1995)]. The procedure requires that the shearing time be much shorter than the materials crystallization time at the chosen temperature. The goal is to study the effect of flow on the nucleation process, not to introduce large crystal during the flow.

The Janeschitz-Kriegl protocol was adapted to extensional flows for this study. Samples were initially heated from room temperature to a temperature of 200°C, 34.4°C above the peak melting temperature of 165.6°C, at a rate of 17.5K/min and held for an additional 5min to erase any thermal and mechanical histories. Although increasing the temperature and soak time would increase the certainty that all of the crystals are fully broken down, these factors lead to undesirable effects such as increased sagging and the likelihood of degradation of the sample. After soaking at 200°C, the samples are then quenched to a temperature that will allow crystallization of the sample. The goal is to study the effect of flow on the nucleation process, not to introduce large crystals during the flow. Therefore, the crystallization temperature must be chosen such that crystallization does not occur during the stretch and also so crystallization can occur in a time that is convenient for testing. The crystallization temperature was chosen to be

$T_c = 146°C$. At this temperature, quiescent crystallization takes approximately 825min and the longest stretch time used in studying changes in percent crystallization was 40s. Note that the imposition of flow accelerates crystallization kinetics and crystallization of the samples was observed to occur shortly after cessation of flow. The samples were quenched at a rate of 5K/min and allowed to equilibrate at $T_c = 146°C$; the total quenching and equilibration time was 15min. At this time, a well-defined extensional strain was applied. The samples were held at the crystallization temperature for an additional 5min; this includes the stretch time so that all samples experience the same temperature profile regardless of the time it takes for the stretch to complete. The midsections of the samples were fully crystallized after this time. However, the portions of the samples near the endplates, which did not experience the same flow history as the midsections, were not crystallized. To be conservative, a second quenching procedure was added to crystallize and solidify the remaining portions of the samples. From the crystallization temperature, the samples were quenched to 127°C at a rate of 2K/min and held for an additional 5min; at this time, the samples were cooled to room temperature and removed from the fixture. To ensure this second cooling step did not affect the final crystallization of the samples, differential scanning calorimetry measurements, which are described in detail in Section 3.3.1, were performed on samples crystallized with the second cooling step and on samples, which were crystallized isothermally at $T_c = 146°C$. No effect on the final percent crystallization was observed as a result of the addition of the second cooling step. Crystallization measurements, which are described in Section 3.3, were performed on samples cut from the middle of the crystallized filament.

CHAPTER 3

RESULTS AND DISCUSSIONS

3.1 Shear Rheometry

The linear viscoelasticity of the polypropylene melts was measured using a commercial rotational rheometer (Stresstech, ATS Rheosystems) with a 25mm diameter parallel plate geometry. Prior to testing, the polypropylene pellets were formed into thin 25mm disks using the hot press. A master curve was compiled of frequency sweeps performed at ten degree increments from 150°C to 210°C. Time-temperature superposition was then used to construct storage modulus, *G'*, and loss modulus, *G''*, curves for the polymer melt at the crystallization temperature, $T_c = 146°\mathrm{C}$. The storage modulus is a measure of the materials elastic response to shear, while the loss modulus is a measure of its viscous response. The master *G'* and *G''* curves and dynamic viscosity, η', curve are characteristic of an entangled polymer melt, refer to Figures 3.1 and 3.2, respectively. The zero-shear-rate viscosity was found to be $\eta_0 = 5.8\times10^4\,\mathrm{Pa\cdot s}$.

The viscoelastic response was used to determine the disengagement time, λ_d, of the polymer at the crystallization temperature, $T_c = 146°\mathrm{C}$. The disengagement time, λ_d, is often estimated as the reciprocal of the frequency at the cross-over point of the *G'* and *G''* curves. Using his method and taking the cross-over to be around $1.8s^{-1}$ (from Figure 3.1) the disengagement time was estimated to be $\lambda_d = 0.56\mathrm{s}$. The problem with this approach to finding the disengagement time is that the cross-over does not occur at a discrete point, rather it occurs over a range of points, as can be seen in Figure 3.1. This is a typical characteristic of polymers which is related to molecular weight distribution

because chains of higher molecular weight display longer relaxation times [Kumaraswamy *et al.* (2002)].

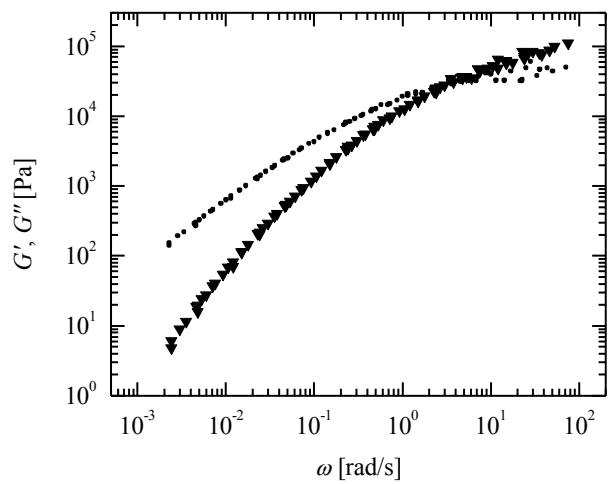

Figure 3.1: The oscillatory shear master curves for polypropylene at T_c = 146°C. Included are the solutions of modulus master curves with storage modulus, *G'* (▼),and loss modulus, *G''*(●).

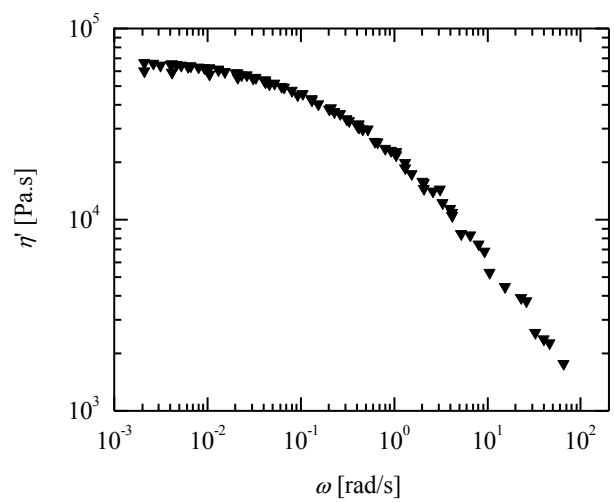

Figure 3.2: The oscillatory shear master curve with dynamic viscosity, η', for polypropylene at T_c = 146°C.

A more accurate method of determining the disengagement time is to fit a multi-mode Maxwell model, which approximates the response of the polymer melt as a set of

viscous dampers and elastic springs, to the data to obtain a spectrum of relaxations times and modulus coefficients. A five-mode Maxwell model was fit to the shear rheology data, using the Iris Rheo-Hub software, to obtain a spectrum of modulus coefficients, G, and relaxation times, λ, which are reported in Table 3.1.

Table 3.1: Spectrum of modulus coefficients and relaxation times for linear polypropylene at T_c = 146°C.

Mode	Modulus Coefficient, G [Pa]	Relaxation Time, λ [s]
1	4.92E+05	6.79E-04
2	7.21E+04	3.69E-02
3	3.39E+04	2.80E-01
4	1.28E+04	1.29E+00
5	3.78E+03	5.45E+00

A viscosity weighted average relaxation time was taken in order to account for the relative importance of each mode. The viscosity weighted average disengagement time is calculated via

$$\lambda_d = \frac{\sum_{i=1}^{n} \lambda_i \eta_i}{\sum_{i=1}^{n} \eta_i}, \tag{3.1}$$

where viscosity is $\eta = \lambda_d G$. Using this method, the disengagement time for the polypropylene used in this study was found to be $\lambda_d = 7.6\text{s}$. This result is in good agreement with measurements performed by Elmoumni *et al.* for various linear polypropylenes [Elmoumni *et al.* (2003)].

The shear rheology was also used to estimate the molecular weight of entanglements, M_e. The molecular weight of entanglements can be found using rubber

elasticity theory, which models polymer chains as entropic springs in a network. Rubber elasticity theory states that the plateau modulus of elasticity, $G_\eta^{\ 0}$, is related to the molecular weight of entanglements by

$$G_\eta^{\ 0} = \frac{\rho RT}{M_e}, \tag{3.2}$$

where $\rho = 0.855\text{g/cm}^3$ is the density for amorphous polypropylene, $R = 8.314\,\text{J/K}\cdot\text{mol}$ is the universal gas constant, and $T = 419\text{K}$ is the temperature at which the plateau modulus is reported [Ferry (1980)]. From Figure 3.1, the plateau modulus of elasticity was estimated to be $G_\eta^{\ 0}$: $4\times10^5\,\text{Pa}\cdot\text{s}$ and the molecular weight of entanglements was found to be on the order of $M_e = 7{,}000\text{g/mol}$.

3.2 Extensional Rheometry

To investigate the effect of extension rate and Weissenberg number on crystallization, the polymer melts were stretched using the Janeschitz-Kriegl protocol, as described in Section 2.4, at extension rates ranging from $0.075\text{s}^{-1} < \dot{\varepsilon} < 0.75\text{s}^{-1}$ to a final strain of $\varepsilon = 3.0$. Extension rates below $\dot{\varepsilon} = 0.075\text{s}^{-1}$ could not be studied because crystallization of the sample was observed to occur during the stretch. Extension rates above $\dot{\varepsilon} = 0.75\text{s}^{-1}$ could not be studied due to excessive diameter decay post stretch as a result of the instability of the fluid filaments developing at high extension rates. This instability is likely due to slipping of highly oriented polymer chains at high Weissenberg numbers. As a result of this instability, extension rates faster than the inverse of the Rouse time ($\lambda_R \sim 0.03\text{s}$) could not be achieved and thus, although alignment of polymer chains is expected, measurements for melts experiencing polymer stretch were not

possible. Hassager *et al*. [Hassager *et al.* (1998)] showed that, using a fast PID control system, measurements beyond the onset of this necking instability could still be made. Unfortunately, the control system used in this study was not fast enough to be employed to explore beyond the onset of necking instability.

Extensional viscosity was found as a function of both extension rate and accumulated Hencky strain for polypropylene melts at 146°C for various extension rates ranging from $0.075\text{s}^{-1} < \dot{\varepsilon} < 0.75\text{s}^{-1}$. Extensional viscosity is plotted as function of accumulated Hencky strain for a variety of extension rates in Figure 3.3. For demonstration purposes, the extensional viscosity measurements in Figure 3.3 are shown for type II experiments because the trends can be seen more clearly than for type III experiments which have a higher variation in data. As accumulated Hencky strain increases, it can be seen from Figure 3.3 that extensional viscosity does not vary monotonically with extension rate.

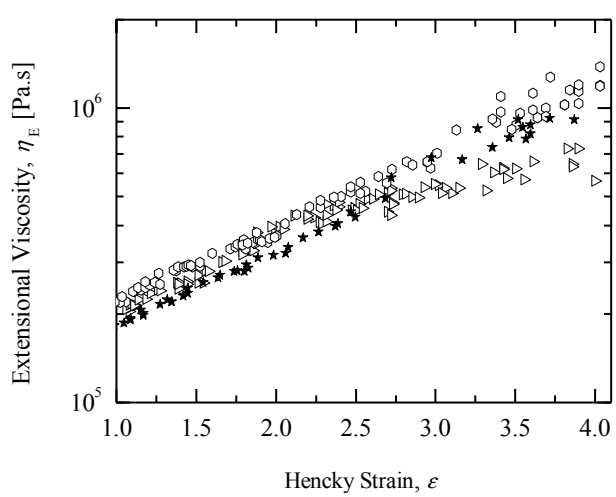

Figure 3.3: Filament stretching extensional rheology measurements of extensional viscosity as a function of accumulated Hencky strain for polypropylene melts stretched at various extension rates at T_c = 146°C. Included are the solutions for extension rates of $\dot{\varepsilon} = 0.11\text{s}^{-1}$ (▷), $\dot{\varepsilon} = 0.15\text{s}^{-1}$ (○), and $\dot{\varepsilon} = 0.38\text{s}^{-1}$ (★).

Extensional viscosity measurements are given as a function of time for a sample of extension rates with the linear viscoelastic limit superimposed over the data in Figure 3.4. For clarity, the measurements in Figure 3.4 are also shown for type II experiments. The linear viscoelastic limit shows the linear extension-rate-independent response of the polymer melt and was calculated via

$$\eta_E(t) = 3\sum_{i=1}^{N} G_i \lambda_i (1 - \exp(-t/\lambda_i)), \tag{3.3}$$

using the spectrum of relation times and modulus coefficients (refer to Table 3.1) extracted from the shear rheology using the multi-mode Maxwell model fits [Larson (1999)].

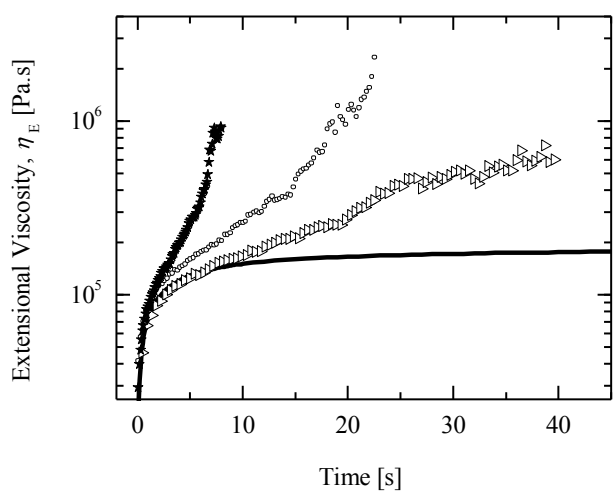

Figure 3.4: Filament stretching extensional rheology measurements of extensional viscosity as a function of time for polypropylene melts stretched at various extension rates at T_c = 146°C. Included are the solutions for extension rates of $\dot{\varepsilon} = 0.11\text{s}^{-1}$ (▷), $\dot{\varepsilon} = 0.15\text{s}^{-1}$ (○), and $\dot{\varepsilon} = 0.38\text{s}^{-1}$ (★). The solid line represents the linear viscoelastic limit.

Modest strain hardening and deviation from the linear viscoelastic limit were observed for all extension rates tested with the deviation occurring at earlier times for increased extension rate. These extensional viscosity results are in agreement with constitutive

models for extensional rheology of entangled linear polymer melts [Bhattacharjee *et al.* (2002)].

In Figure 3.5, a closer look at the relationship between extensional viscosity and extension rate shows that the polymer melt exhibits some degree of extensional thickening up to a critical extension rate, $\dot{\varepsilon} = 0.10 s^{-1}$, after which there is a transition to extensional thinning.

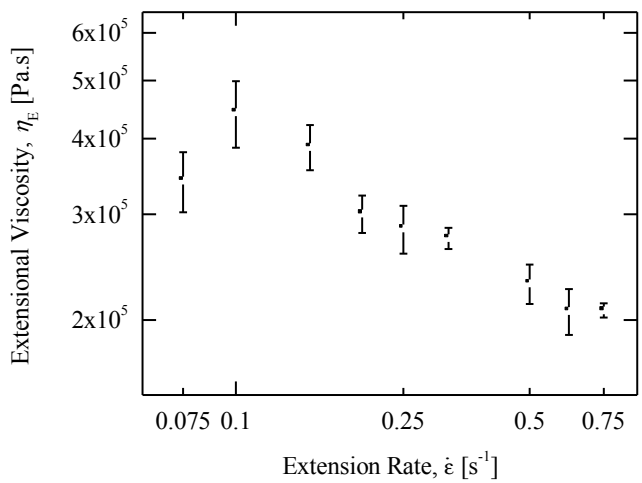

Figure 3.5: Filament stretching extensional rheology measurements of extensional viscosity as a function of extension rate for polypropylene melts stretched at T_c = 146°C to a fixed strain of $\varepsilon = 3.0$.

The extensional viscosity does not reach steady-state due to instability of the fluid filaments at high strains. For this reason, extensional viscosity is reported at an accumulated strain of $\varepsilon = 3.0$. In addition, the extensional viscosity measurements at this strain are of importance as this is the strain which was chosen for the crystallization experiments.

For entangled polymer systems, at Weissenberg numbers greater than $Wi > ½$, the flow has become strong enough to align tubes of constrained polymer chains and

extensional thinning is observed as a result [Bhattacharjee *et al.* (2002)]. Plotting Trouton ratio as a function of Weissenberg number, as done in Figure 3.6, can often be more insightful than simply looking at extensional viscosity versus extension rate.

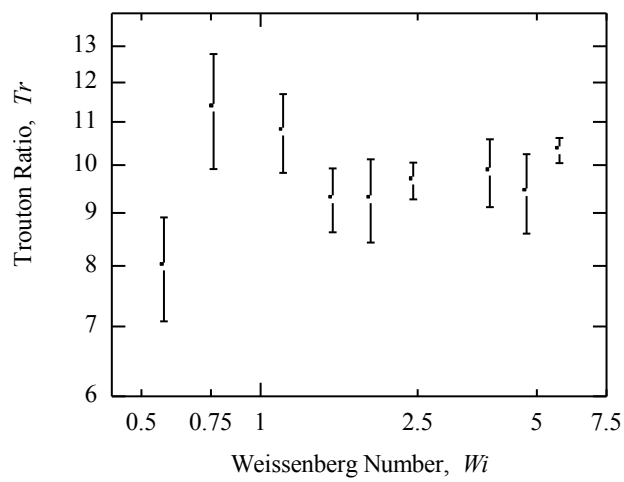

Figure 3.6: Filament stretching extensional rheology measurements of Trouton ratio as a function of Weissenberg number for polypropylene melts stretched at T_c = 146°C to a fixed strain of $\varepsilon = 3.0$.

The Trouton ratio is observed to reach a maximum for Weissenberg numbers in the range of $1/2 < Wi < 1$, after which some degree of extensional thinning is observed. As the Weissenberg number continues to increase, the Trouton ratio appears to reach a plateau. The results suggest that the flow is not causing significant deformation of the polymer chains within the tubes of constrained polymer because of the absence of significant extensional thickening at high Weissenberg numbers [Rothstein and McKinley (2002a)]. The trends in extensional viscosity, and consequently Trouton ratio, provide information about the deformation and alignment which is induced by the flow. These trends are found to play a significant role in the crystallization behavior of polypropylene, as will be shown by the results in the following sections.

3.3 Crystallization Measurements

The final percent crystallization of the samples was characterized as a function of extension rate using differential scanning calorimetry (DSC). Polarized-light microscopy and small angle X-ray scattering (SAXS) were used to investigate changes in the final crystal size and structure as a result of the application of extensional flows of varying strengths. The methods used, how they were applied to the study of polymer crystallization, and the results are described in the following sections.

3.3.1 Differential Scanning Calorimetry

Differential scanning calorimetry measures the heat absorbed or released from a sample as it is heated or cooled. DSC was performed on the crystallized polypropylene samples to determine the final percent crystallization using a TA Instruments model DSC 1000. All experiments were performed under purged nitrogen and samples were heated from 25°C to 200°C. The samples were first heated at a rate of 10K/min up to 100°C. A slower rate of 1K/min was used from 100°C to 200°C, as this is the temperature range of most interest. DSC measurements were performed on the polypropylene samples post-stretch and crystallization to determine the degree of crystallinity. The results were compared to DSC measurements of quiescent samples, which experienced the same thermal history as the stretched samples in the absence of extensional flow. In Figure 3.7, two DSC measurements are presented, one for a quiescent case, the other for an extension rate of $\dot{\varepsilon} = 0.25\text{s}^{-1}$. In this case, the energy required to melt the stretched sample was found to be significantly larger than the energy required to melt the quiescent sample. The energy released from a sample, as it is melted, provides information about the

crystallization. As the percent crystallization increases, more energy is required to melt the sample.

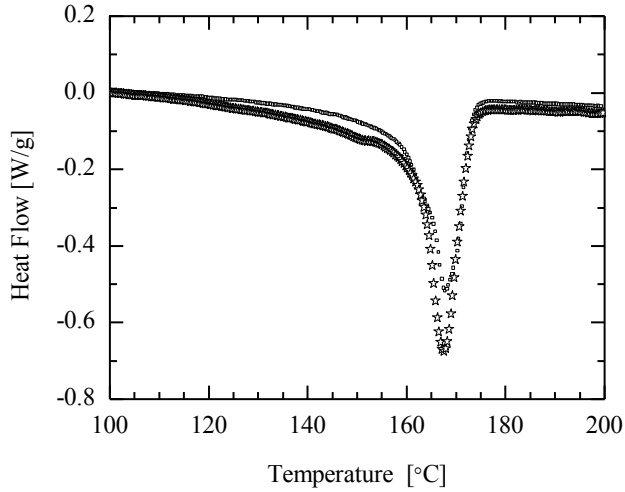

Figure 3.7: DSC measurements showing with heat flow as a function of temperature. Included are polypropylene samples crystallized under quiescent conditions (□) and following a stretch with an extension rate of $\dot{\varepsilon} = 0.25s^{-1}$ at a fixed strain of $\varepsilon = 3.0$ (✯).

The area enclosed by the melt curve gives the latent heat of fusion, ΔH, of the sample, which is used to calculate percent crystallization. The percent crystallization is calculated from the DSC data as $\Delta H / \Delta H_u$, where $\Delta H_u = 209\text{J/g}$ [Quirk and Alsamarraie (1989)] is the heat of fusion per unit mass for complete crystallization of polypropylene.

Percent crystallization is reported in Figure 3.8 as a function of extension rate and Weissenberg number for samples stretched to a final strain of $\varepsilon = 3.0$ as well as for quiescent samples. Percent crystallization begins to increase from the quiescent state at the critical extension rate of $\dot{\varepsilon} = 0.10\text{s}^{-1}$ and continues to increase to a maximum at the peak extension rate $\dot{\varepsilon} = 0.25\text{s}^{-1}$. This maximum of 52% crystallinity represents an increase of approximately 18% above the quiescent case. A similar maximum was observed by Chellamuthu *et al.* [Chellamuthu *et al.* (In Press 2011)] for two different

poly-1-butene samples. Thus it appears that this phenomenon is not characteristic of only poly-1-butene and may prove to be a robust phenomenon independent of the polymer and its degree of polydispersity. After the maximum, the percent crystallization decreases to a plateau which is only slightly more crystalline than the quiescent case.

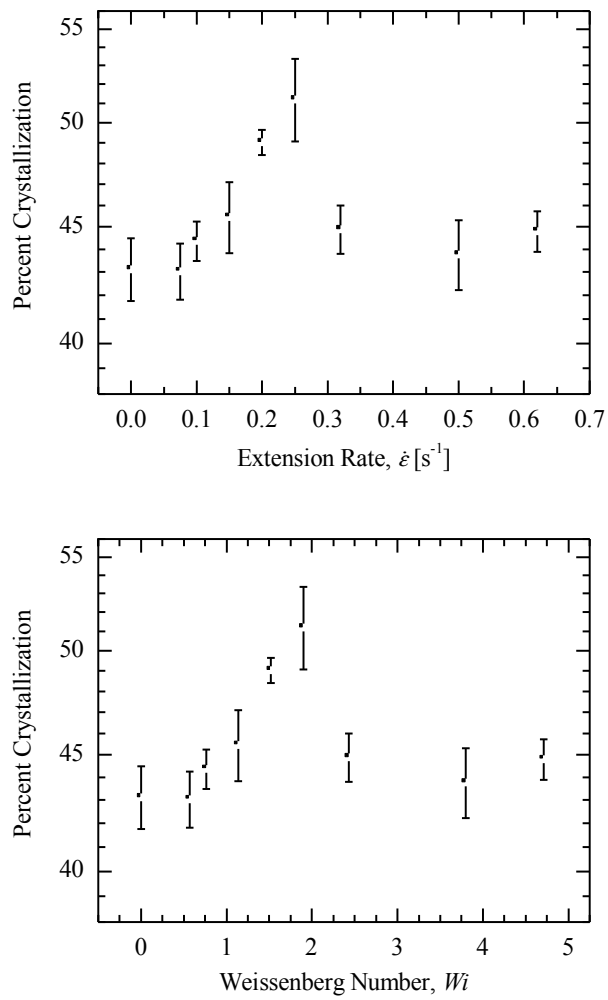

Figure 3.8: Percent crystallization as a function of extension rate and Weissenberg number for polypropylene samples crystallized following stretches to a fixed strain of $\varepsilon = 3.0$.

When the extension rate is rewritten as a Weissenberg number, the increase in percent crystallization is observed to begin at a Weissenberg number of $Wi = 1$ and continues to a

maximum at $Wi = 2$. This initial onset of increase in percent crystallization at $Wi = 1$ was also observed by Chellamuthu *et al.* [Chellamuthu et al. (In Press 2011)].

3.3.1.1 Peak Melting Temperature

DSC was also used to examine the changes in peak melting temperature as a result of increasing extension rate. The trends in peak melting temperature can provide information about the final crystal size and structure of a polymer sample. Increased molecular stretch, as present in a shish-kebab structure, results in a decreased entropy state and therefore an increase in melting temperature from the quiescent case [Keller and Kolnaar (1997)]. On the other hand, a decrease in melting temperature is indicative of the increased stretch of tubes of constrained polymer chains as well as smaller spherulites which are easier to break down than large crystals and more random in orientation as a result of their packing characteristics. The peak melting temperatures of polypropylene samples are shown as a function of extension rate in Figure 3.9.

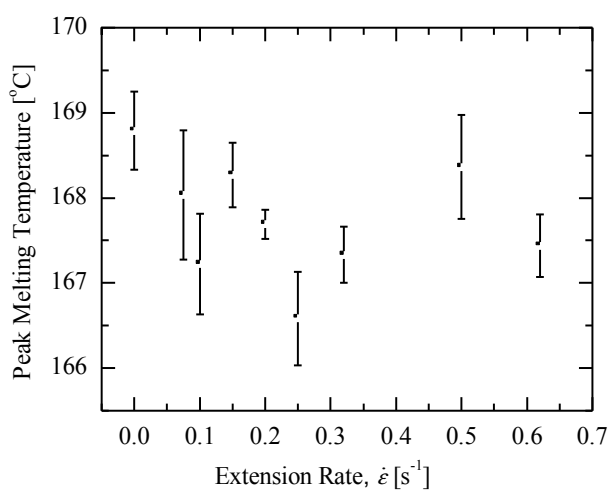

Figure 3.9: Peak melting temperature as a function of extension rate for polypropylene samples crystallized following stretches of various extension rates to a fixed strain of $\varepsilon = 3.0$.

A general downward trend was observed in the peak melting temperature with increasing extension rate until the peak extension rate, as shown in Figure 3.9. This may suggest an increase in polymer stretch as a result of the increase in strength of the extensional flow and also suggests a decrease in spherulite size. However, no clear conclusions can be drawn from the measurements of peak melting temperature however, as the variation in the data is great enough to obscure any inferred trends.

3.3.1.2 Time-Temperature Transformation

Isothermal DSC experiments were also performed to determine the dependence of the rate of crystallization of polypropylene on temperature. All isothermal crystallization experiments were performed in the DSC under purged nitrogen. Samples were heated to 200°C at a rate of 10K/min and allowed to equilibrate in order to erase any thermal or mechanical history. The samples were then quickly quenched to various crystallization temperatures at a rate of 10K/min and held at that temperature. The time for crystallization to begin and complete, after the crystallization temperature was reached, was measured from the crystallization curves constructed from the DSC measurements. Isothermal crystallization experiments were performed at temperatures ranging from 130°C to 150°C. Below 130°C, the sample began to crystallize before reaching the set crystallization temperature. Experiments above 150°C were not performed because of the long times required for crystallization to complete at high temperatures. An isothermal crystallization curve is shown in Figure 3.10 for polypropylene at 145°C. The times for crystallization to begin and complete at 145°C were found to be approximately 27min and 735min, respectively. The time-temperature transformation diagram, Figure 3.11, provides information about the rate of crystallization over a range of temperatures.

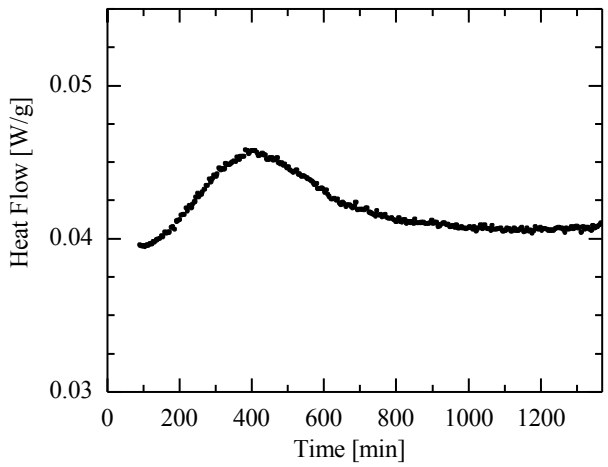

Figure 3.10: DSC measurements showing heat flow as a function of time for polypropylene crystallizing isothermally at 145°C.

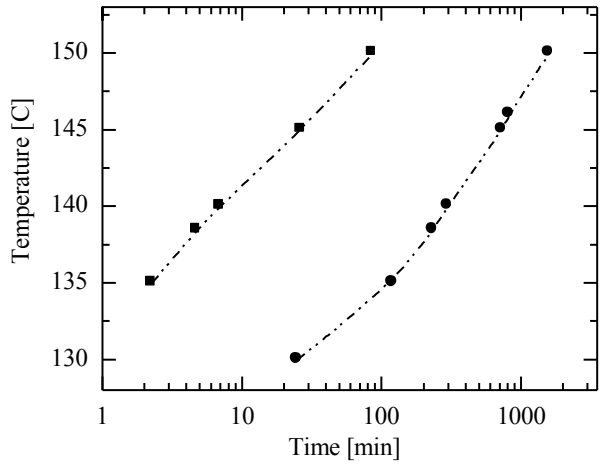

Figure 3.11: Time-temperature transformation diagram for polypropylene. Included are the results for the onset (■) and completion of crystallization (●).

As temperature is increased, the time for crystallization to begin increases slightly and the rate of crystallization is decelerated greatly. It can be seen from Figure 3.11, that at a crystallization temperature of 146°C, it takes approximately 30min for polypropylene to begin crystallization and approximately 825min for crystallization to complete.

3.3.2 Polarized-Light Microscopy

Optical microscopy (Nikon TE200-U) was performed through crossed polarizers to qualitatively characterize changes in spherulite size, numbers and crystalline structure as a result of the application of extensional flow. The crystal structure can be observed by placing a sample between two polarizers which are oriented 90° to each other. Light that is normal to the polarizers is blocked while light that is refracted by the crystals is advanced, allowing the morphology to become distinguishable. Spherulitic crystals appear in the polarized microscopy images as Maltese crosses, as shown in Figure 3.12.

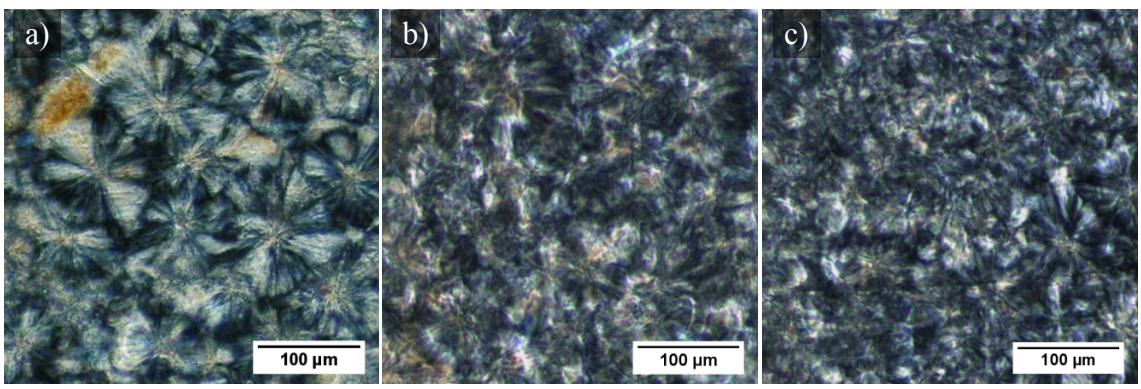

Figure 3.12: Microscopy images taken through crossed polarizers of polypropylene samples showing the size of spherulites under a) quiescent conditions and following stretches with extension rates of b) $\dot{\varepsilon} = 0.10\text{s}^{-1}$ and c) $\dot{\varepsilon} = 0.25\text{s}^{-1}$ at a fixed strain of $\varepsilon = 3.0$. The direction of flow is aligned vertically.

The microscopy images show an increase in the number of spherulites and the decrease in spherulite size with increasing extension rate up to the peak extension rate, $\dot{\varepsilon} = 0.25\text{s}^{-1}$. This observation suggests an increased nucleation density with increased extension rate. No change in spherulite size or number was observed from the quiescent case for extension rates below the critical extension rate, $\dot{\varepsilon} = 0.10\text{s}^{-1}$. After the peak extension rate, changes to spherulite size and numbers appeared to cease. No signs of a highly

oriented shish-kebab structure in the flow direction could be inferred from the microscopy images. Thus, scattering measurements were required to determine the final crystalline structure.

3.3.3 Small Angle X-ray Scattering

Small angle X-ray scattering was also performed on the samples to investigate the effect of extensional flow on the structure and alignment of the polymer crystals. When X-rays are passed through a sample, they are scattered in a way which is dependent on their interaction with crystals and amorphous material in the sample. An illustration of small angle X-ray scattering and the corresponding two-dimensional scattering patterns for spherulitic (isentropic) and oriented crystal structures are shown in Figure 3.13.

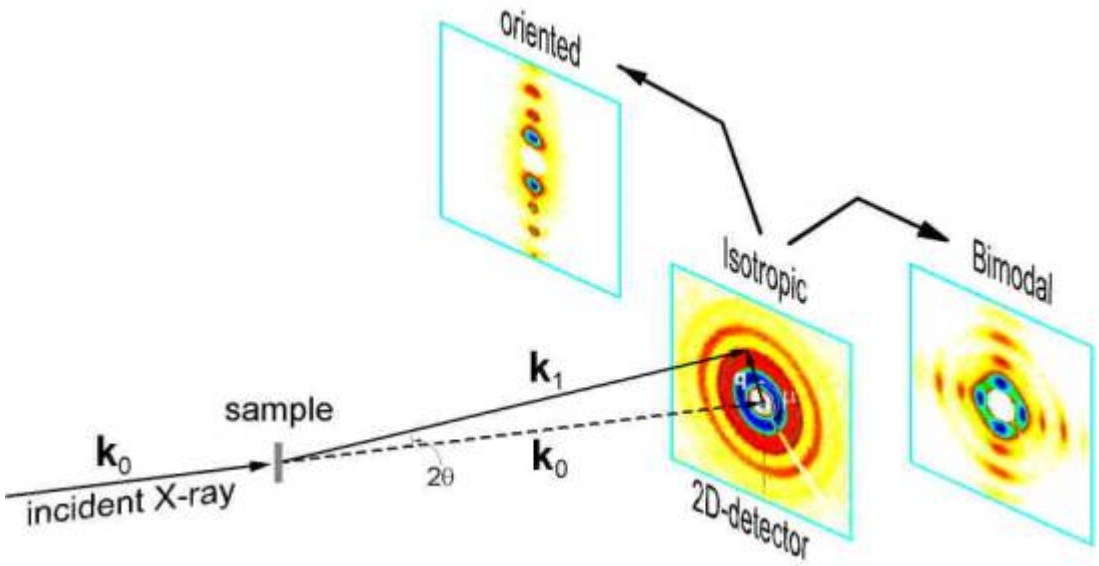

Figure 3.13: Small angle X-ray scattering and two-dimensional scattering patterns [Wiesner (2008)].

If a regular structure were to exist, diffracted X-rays would interfere with each other resulting in maxima in the scattering intensity [Lyngaae-Jsrgensen and Sondergaard

(1995)]. For a lamellar structure, the two-dimensional scattering pattern will be azimuthally symmetric and the lamellae appear as rings. If an aligned shish-kebab structure exists, X-rays are scattered perpendicular to the direction of alignment and "equatorial steaks" appear in the two-dimensional scattering patterns [Samon *et al.* (1999)].

In addition to two dimensional scattering patterns, the scattering intensity, I, as a function of the wave vector, q, can also be obtained from SAXS measurements. The scattering vector is defined as $q = k_0 - k_1$, where k_0 and k_1 are the wave vectors tangent to the incident and scattered x-rays, respectively [Lyngaae-Jsrgensen and Sondergaard (1995)]. For a lamellar crystal structure, the scattering intensity peaks occur at scattering vector magnitudes of $q_n = q_0 n$, where q_0 is the position of first peak and n=1,2,etc. [Chu and Hsiao (2001)].

SAXS measurements were performed using an instrument from Molecular Metrology Inc. (Rigaku S-Max3000). The X-ray beam was 0.40mm in diameter with a wavelength of $\lambda = 0.1542\text{nm}$. The sample to detector distance was calibrated using silver behenate standard peak at wave vector of $q = 1.076\text{nm}^{-1}$, where $q = (4\pi/\lambda)\sin\theta$ and 2θ is the scattering angle. The samples were placed in the instrument such that measurement was taken at the axial center of the filament and the flow direction was aligned perpendicular to the beam direction; this allows any crystal alignment in the flow direction to be detected in the two-dimensional scattering patterns.

SAXS was performed for a number of samples for each extension rate examined. Several characteristic scattering patterns and scattering intensity versus wave vector, q,

are shown for an extension rate below and an extension rate above the critical extension rate in Figures 3.14 and 3.15, respectively.

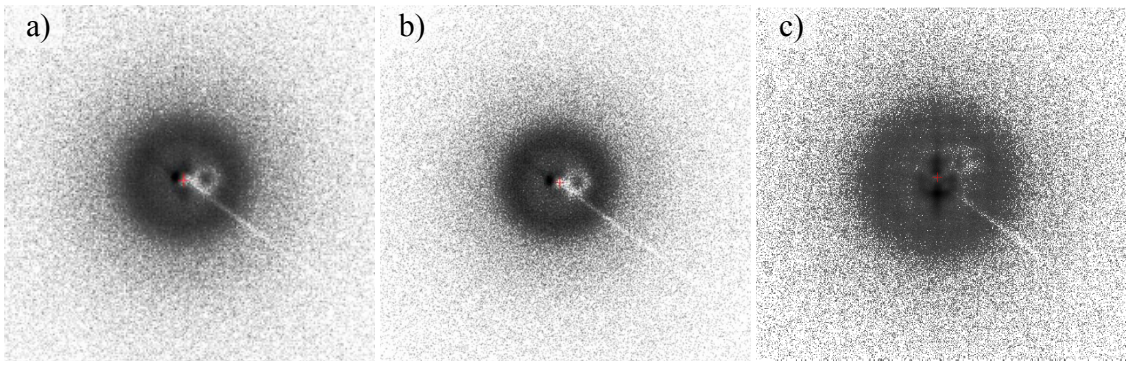

Figure 3.14: Two-dimensional small angle X-ray scattering patterns for polypropylene samples crystallized following stretches with extension rates of a) $\dot{\varepsilon} = 0.075\text{s}^{-1}$ and b) $\dot{\varepsilon} = 0.25\text{s}^{-1}$ to a final strain of $\varepsilon = 3.0$ and an extension rate of c) $\dot{\varepsilon} = 0.25\text{s}^{-1}$ to a final strain of $\varepsilon = 4.0$. The stretch direction is aligned horizontally to the scattering patterns.

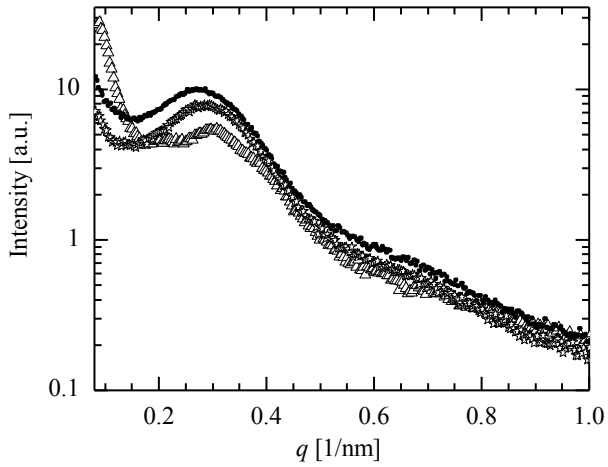

Figure 3.15: Intensity of the scattering images presented in Figure 10 as a function of scattering vector, *q*, for polypropylene samples crystallized following stretches with extension rates of $\dot{\varepsilon} = 0.075\text{s}^{-1}$ (•) and $\dot{\varepsilon} = 0.25\text{s}^{-1}$ (△) to a final strain of $\varepsilon = 3.0$ and an extension rat of $\dot{\varepsilon} = 0.25\text{s}^{-1}$ (✯) to a final strain of $\varepsilon = 4.0$.

All of the scattering patterns showed equally spaced axisymmetric rings, which are indicative of a lamellar crystal structure. The d-spacing, or distance between lamellar layers, the was measured to decrease slightly from 23nm to 22nm between extension

rates of $\dot{\varepsilon} = 0.075\text{s}^{-1}$ and $\dot{\varepsilon} = 0.25\text{s}^{-1}$, respectively. The maximum effect on d-spacing was found to occur at the transition to the critical extension rate where a large increase in crystallization was observed. Little or no effect was observed between extension rates above the critical extension rate.

3.4 Extensional-Flow-Induced Crystallization with Varying Strain

Flow-induced crystallization can be affected by the degree of strain applied in addition to strain rate. By applying the Janeschitz-Kriegl protocol for a range of strains at select extension rates, the effect of varying strain can be characterized. It has been shown that in order for shear induced shish-kebab formation to occur, a critical shear rate and shear strain must be applied [Van Puyvelde *et al.* (2008)]. Although much smaller strains are required in extension to produce a shish-kebab structure, a critical strain may still be required in extension. An extension rate of $\dot{\varepsilon} = 0.25\text{s}^{-1}$, for which the maximum percent crystallization was observed at a strain of $\varepsilon = 3.0$, was chosen to examine the changes in percent crystallization as a result of varying strain in the range of $\varepsilon = 2.0$ to $\varepsilon = 4.0$ and to determine if an increase in strain would lead to the formation of a shish-kebab crystal structure. In addition, strains were applied in the range of $\varepsilon = 3.0$ to $\varepsilon = 4.0$ for an extension rate of $\dot{\varepsilon} = 0.075\text{s}^{-1}$, for which no change in crystallization was observed from the quiescent state at a strain of $\varepsilon = 3.0$, to investigate if an increase in strain would lead to an increase in crystallization. The magnitude of accumulated strain was limited to $\varepsilon = 4.0$ for both extension rates, due to instabilities that ensued at high strains and the limits of the PID control system.

For both extension rates, a modest increase in crystallization of a couple percent was observed with increasing extensional strain, however, in neither case was the trend significant when compared to the uncertainty in the data, refer to Figure 3.16.

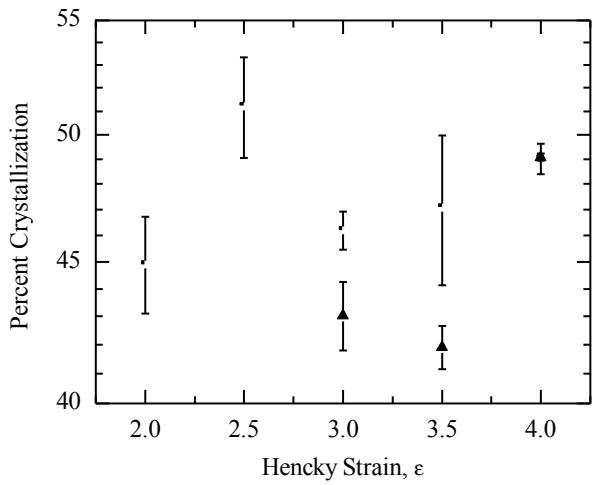

Figure 3.16: Percent crystallization as a function of final Hencky strain for polypropylene samples crystallized following stretches with extension rates of (▲) $\dot{\varepsilon} = 0.075\text{s}^{-1}$ and (■) $\dot{\varepsilon} = 0.25\text{s}^{-1}$.

Additionally, SAXS measurements showed that even at a strain of $\varepsilon = 4.0$, neither extension rate resulted in the creation of shish-kebabs. Furthermore, no significant change in the scattering patterns or effect on d-spacing was observed as a result of increase in strain, refer to Figures 3.13 and 3.14.

3.5 Crystallization Time Measurements

In order to better understand the crystallization dynamics under extensional flow, the time required for crystallization to occur during flow was directly measured for polypropylene. By stretching the polypropylene melts for times much greater than prescribed by the Janeschitz-Kriegl protocol and observing crystallization, insight can be gained into the rate of crystal nucleation and growth under extensional-flow-enhanced

crystallization. In the experiments, the time of crystallization was marked by the time at which a sudden increase in the measured force was observed. This approach was similar to that used by Hadinata *et al.* [Hadinata *et al.* (2007)] for poly-1-butene, where they defined crystallization time to be the time at which a sharp increase in extensional viscosity was observed during stretching of the polymer melts.

Polypropylene samples were stretched at extension rates ranging from $\dot{\varepsilon} = 0.01\text{s}^{-1}$ to $\dot{\varepsilon} = 0.15\text{s}^{-1}$ for accumulated Hencky strains that in some cases grew in excess of $\varepsilon = 10.0$. For a number of reasons, including the fluctuating forces which ensue as a result of the applied velocity profile, these experiments could not be performed easily using the PID controller. As a result, an exponential velocity (or type II) profile was imposed on the end plates instead and the resulting extension rate imposed on the fluid filament was calculated from the radius decay as described by Equation 2.1. The range of extension rates which could be investigated was limited by sagging of the melts under gravity at extension rates below $\dot{\varepsilon} = 0.01\text{s}^{-1}$ and by failure of the fluid filaments before crystallization could occur caused by the necking instability at high strains for extension rates above $\dot{\varepsilon} = 0.15\text{s}^{-1}$.

In Figure 3.17, the measured force is presented as a function of time. A sudden increase in force can be seen towards the end of the stretch; this jump in force and consequential jump extensional viscosity was taken to be the crystallization time. The onset of crystallization is observed as an abrupt upturn in the force measurement at roughly 40s and 60s for extension rates of $\dot{\varepsilon} = 0.10\text{s}^{-1}$ and $\dot{\varepsilon} = 0.15\text{s}^{-1}$, respectively. The crystallization time is shown for various extension rates in Figure 3.18. The crystallization time was observed to decrease linearly with one over extension rate. A

similar trend and dependency on extension rate was observed by Hadinata *et al.* [Hadinata *et al.* (2007)]. This indicates that the dynamics of crystallization are dictated by the strength of the flow.

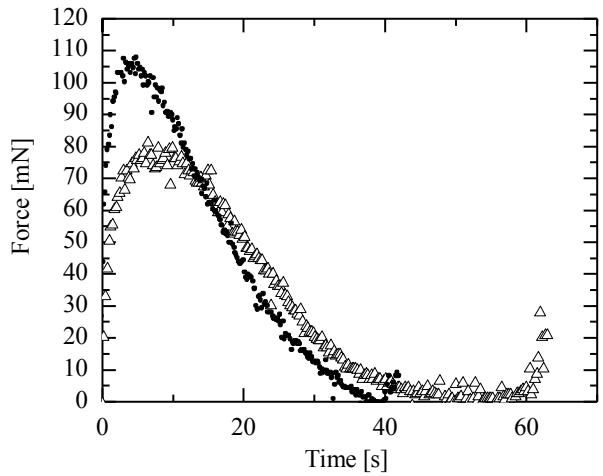

Figure 3.17: Filament stretching extensional rheology measurements of force as a function of time for polypropylene samples crystallizing during extensional flows with extension rates of $\dot{\varepsilon} = 0.10\text{s}^{-1}$ (△) and $\dot{\varepsilon} = 0.15\text{s}^{-1}$ (•) at T_c = 146°C.

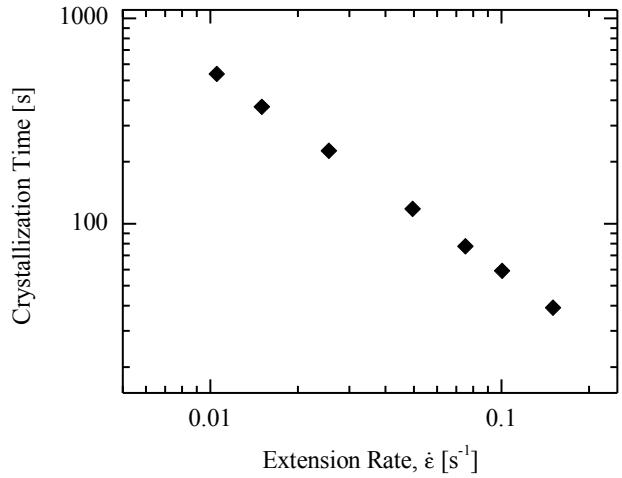

Figure 3.18: Crystallization time as a function of extension rate for polypropylene.

Even at low extension rates where flow-induced crystallization is not found to enhance the final crystalline state or percent crystallization, flow appears to increase the rate of

nucleation by increasing the frequency of collisions between polymer chains and the opportunity for crystallization well beyond what would occur through diffusion alone.

3.6 Flow-Induced Crystallization of Branched Polypropylene

Branched polymers or blends of branched and linear polymers are often used in place of linear polymers for the manufacturing of products because of their higher melt strength [Yu *et al.* (2009)]. In many cases, the presence of branched chains can lead to an increase in the degree of crystallinity and therefore, superior mechanical properties [Agarwal *et al.* (2003); Yu *et al.* (2009)]. In addition, branched polymers tend to have faster crystallization kinetics. Through in situ rheo-SAXS and –WAXD measurements, Agarwal *et al.* [Agarwal *et al.* (2003)] demonstrated that, under shear flow, the crystallization of branched polypropylene was an order of magnitude faster than for linear polypropylene. They also found that the branched polypropylene contained a much greater fraction of crystals with an oriented shish-kebab morphology.

Tabatabaei *et al.* [Tabatabaei *et al.* (2009)] recently studied the effect of concentration of branched chains in linear polypropylene. They found that increasing the concentration of branching led to an increase in the number of crystals and the speed of crystallization kinetics. They attributed these phenomena to instantaneous and heterogeneous nucleation brought on by the presence of branched chains. More interestingly, their results showed an increase in percent crystallization up to a critical concentration, followed by a decrease. The initial increase was a result of the increase in nucleation sites caused by the presence of branched chains. However, at a certain concentration the decrease in chain mobility caused by the addition of branched chains

outweighed the benefit of increased nucleation sites and resulted in a decrease in percent crystallization. [Tabatabaei *et al.* (2009)]

3.6.1 Materials

Long-chain branched polypropylene (LCBPP) samples were prepared in the same fashion as for linear polypropylene. The LCBPP, WB140HMS, was also provided from Borealis in the form of pellets. WB140HMS has a molecular weight of $M_w = 350,000\text{g/mol}$ and a polydispersity of 6.0. The entanglement molecular weight is on the order of $M_e = 7,000\text{g/mol}$.

3.6.2 Shear Rheology

The linear viscoelasticity of the LCBPP was measured using the same methods as was used with the linear polypropylene melts, as described in Section 3.1. The master *G'* and *G"* curves and dynamic viscosity curve are reported at a temperature of 150°C in Figures 3.19 and 3.20, respectively. The results are typical of branched polymers which display stronger shear thinning than their linear counterparts [Tabatabaei *et al.* (2009)]. Furthermore, the presence of long-chain branches results in an increase in the elasticity of the polymer. It can be seen from Figure 3.19, that the plateau storage modulus of LCBPP is a couple orders of magnitude greater than that of the linear polypropylene, although the shear rheology experiments were not performed at high enough frequencies to actually observe the plateau.

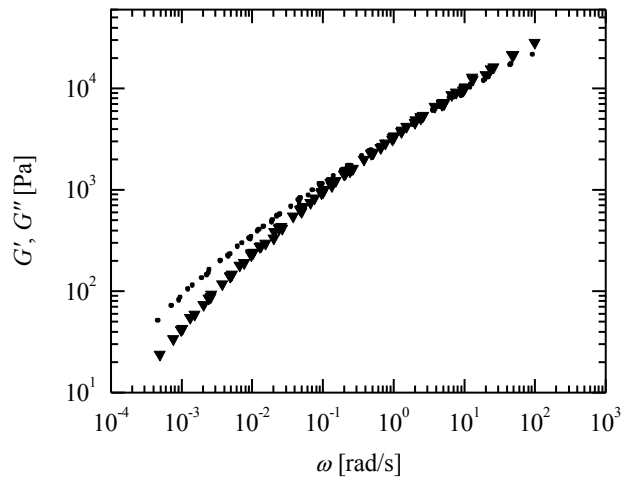

Figure 3.19: The oscillatory shear master curves for LCBPP at 150°C. Included are the solutions of modulus master curves with storage modulus, *G'* (▼), and loss modulus, *G"*(●).

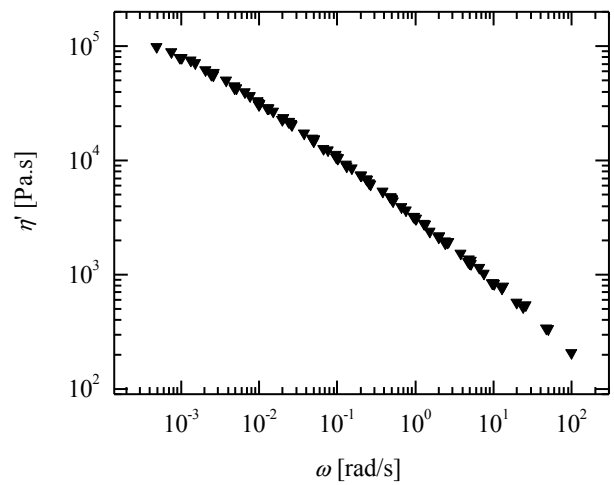

Figure 3.20: The oscillatory shear master curve with dynamic viscosity, η', for LCBPP at 150°C.

A seven-mode Maxwell model was fit to the shear rheology of the LCBPP to determine the disengagement time of the LCBPP melt. The spectrum of modulus coefficients, G, and relaxation times, λ, are reported in Table 3.2 for LCBPP. The viscosity weighted average disengagement time was calculated to be on the order of

$\lambda_d = 80s$. The order of magnitude difference between the disengagements time for LCBPP and linear polypropylene is a result of the presence of long-chain branches which affect the relaxation of stress in the polymer melt [Tabatabaei *et al.* (2009)].

Table 3.2: Spectrum of modulus coefficients and relaxation times for LCBPP at 150°C.

Mode	Modulus Coefficient, G [Pa]	Relaxation Time, λ [s]
1	8.27E+04	1.73E-03
2	1.65E+04	2.23E-02
3	6.52E+03	1.15E-01
4	2.94E+03	5.07E-01
5	1.55E+03	1.94E+00
6	7.75E+02	8.22E+00
7	3.81E+02	3.19E+01

3.6.3 Extensional-Flow-Induced Crystallization Experiments

Experiments starting by identifying a range of temperatures for which the Janeschitz-Kriegl protocol could be applied to the LCBPP. Crystallization time experiments were performed to characterize the crystallization dynamics of LCBPP under extensional flow and to identify the temperatures at which the LCBPP would crystallize during flow after large strains had been applied. These experiments allow the limits of temperature and stain to be identified for the Janeschitz-Kriegl protocol.

Samples were initially heated from room temperature to a temperature of 200°C, 36.7°C above the peak melting temperature of 163.3°C, at a rate of 17.5K/min and held for an additional 5min to erase any thermal and mechanical histories. The samples were then quenched to a crystallization temperature at a rate of 5K/min and then allowed to equilibrate. Though trial and error, the range of workable temperatures for the crystallization time experiments was identified to be between 148°C and 155°C.

Temperatures below 148°C resulted in crystallization of the samples either before equilibration or in a time which was too short to allow for stretches to be performed. Temperatures over 155°C were too close to the peak melting temperature to be certain that any flow-induced crystallization would not be erased during the experiment.

3.6.4 Results and Discussions

The LCBPP samples were stretched at extension rates ranging from $0.01\text{s}^{-1} \leq \dot{\varepsilon} \leq 0.25\text{s}^{-1}$ at various temperatures in the identified workable range. At low extension rates, the samples pulled out of the top plate as a result of the high elasticity of LCBPP. At high extension rates, the samples were not observed to crystallize during stretch, even for strains in excess of $\varepsilon = 10.0$. The accumulated strains which could be obtained were limited by the height of the extensional rheometer. None of the samples tested were observed to crystallize during stretch, even at low temperatures, where quiescent crystallization occurred shortly after equilibration. The observations from the flow-induced-crystallization time experiments suggest that the application of extensional flow hinders crystallization of long-chain branched polypropylene. Further investigation is needed to characterize the crystallization of LCBPP under extensional flow and the causes for the impedance of crystallization.

CHAPTER 4

CONCLUSIONS

The degree of crystallization of polypropylene was found to be strongly affected by the application of extensional flow. A critical extension rate was found to be required for an increase in crystallization to occur. At this critical extension rate, the Weissenberg number had reached $Wi = 1$ and the flow was strong enough to align the tubes of constrained polymer chains. The critical extension rate corresponds to the maximum Trouton ratio, which verifies the occurrence of alignment and deformation of tubes of constrained polymer chains in the flow direction. Percent crystallization increased to a maximum, which was 18% greater than the quiescent case, at the peak extension rate. After the maximum, the percent crystallization decreased to a plateau. In this region the percent crystallization was a few percent greater than the quiescent case. Polarized light microscopy verified an increase in the number of spherulites and decrease in spherulite size for extension rates at or above the critical extension rate. Microscopy also showed a continued increase in number and decrease in size of spherulites until the peak extension rate at which the maximum percent crystallization occurs. No apparent change in spherulite size or number was observed for extension rates above the peak extension rate.

Small angle X-ray scattering was used to investigate the crystal structure of the stretched polypropylene samples. The scattering patterns of all of the samples examined displayed a lamellar crystal structure which is indicated by an azimuthally symmetric scattering pattern with radially spaced bright rings. A 7% decrease in d-spacing was observed at the transition to the critical extension rate. Inter-lamellar spacing was not

found to be greatly influenced by the strength of flow as it was not observed to change for an increase in extension rate past the critical extension rate.

The trends in percent crystallization for varying extension rates are similar to those found by Chellamuthu *et at.* for poly-1-butene [Chellamuthu *et al.* (In Press 2011)], even though a shish-kebab structure was not detected for any of the samples in the SAXS measurements or polarized light microscopy images. This suggests that the maximum in percent crystallization is not dependant on the formation of a shish-kebab crystal structure, as suggested by Chellamuthu *et al.* [Chellamuthu *et al.* (In Press 2011)], but is a more general result for a wide spectrum of polymers. It is interesting to note, however, that the plateau in percent crystallization for poly-1-butene, which possessed a shish-kebab crystal structure, was still 10-20% greater than the quiescent case [Chellamuthu *et al.* (In Press 2011)]. However, the plateau in percent crystallization for polypropylene, which did not possess a shish-kebab crystal structure, was only a few percent greater than the quiescent case. These results suggest that in some cases the formation of a shish-kebab crystal structure can lead to a greater degree of crystallinity in the final state.

The onset of crystallization for polypropylene was also studied. The onset of crystallization time, t_c, was found to be proportional to the inverse of extension rate, $t_c \propto \dot{\varepsilon}^{-1}$. This coupling demonstrates the strong dependence of crystallization time on the extension rate. The results display the same trend as those reported by Hadinata *et al.* for poly-1-butene [Hadinata *et al.* (2007)]. The decrease crystallization time with increasing extension rate can be attributed to the reduction in the kinetic barrier for crystallization resulting from alignment of the polymer chains as well as the increased interaction between polymer chains induced by flow.

Interestingly, the decrease in the crystallization time was observed for extension rates well below the critical extension rate, where no increase in percent crystallization from the quiescent state was observed. This indicates that even for flows which do not result in an increase in crystallization, the kinetics of crystallization are strongly influenced by the application of extensional flow. In these cases the flow is not strong enough cause alignment or deformation of the polymer chains since the time scale of the flow is long in comparison to the relaxation time of the polymer melt. The decrease in crystallization time is therefore likely due to the enhanced interaction between polymer chains as they are advected in the imposed extensional flow.

BIBLIOGRAPHY

Agarwal, P. K., Somani, R. H., W. Weng, A. M., L. Yang, S. R., L. Liu and Hsiao, B. S. "Shear-induced crystallization in novel long chain brached polypropylene by in situ rheo-saxs and -waxd," Macromolecules **36**, 5226-5235 (2003).

Anna, S. L., McKinley, G. H., Nguyen, D. A., Sridhar, T., Muller, S. J., Huang, J. and James, D. F. "An inter-laboratory comparison of measurements from filament stretching rheometers using common test fluids," J. Rheol. **45**, 83-114 (2001).

Anna, S. L., Rogers, C. B. and McKinley, G. H. "On controlling the kinematics of a filament stretching rheometer using a real-time active control mechanism," J. Non-Newtonian Fluid Mech. **87**, 307-335 (1999).

Bassett, D. C. *Principles of polymer morphology - (cambridge solid state science series)* (Press Syndicate of the University of Cambridge, Oxford, 1981).

Belyi, V. A. a. G. G. P. "The effects of stabilizers and fillers on the adhesional properties of polypropylene," International chemical engineering **11**, 89-93 (1971).

Bhattacharjee, P. K., Oberhauser, J., McKinley, G. H., Leal, L. G. and Sridhar, T. "Extensional rheometry of entangled solutions," Macromol. **35**, 10131-10148 (2002).

Chellamuthu, M., Arora, D., Winter, H. H. and Rothstein, J. P. "Extensional flow induced crystallization of isotactic poly-1-butene using a filament stretching rheometer," Journal of Rheology (In Press 2011).

Chu, B. and Hsiao, B. S. "Small-angle x-ray scattering of polymers," Chemical Reviews **101**, 1727-1761 (2001).

Elmoumni, A. and Winter, H. H. "Large strain requirements for shear-induced crystallization of isotactic polypropylene," Rheologica Acta **45**, 793-801 (2006).

Elmoumni, A., Winter, H. H., Waddon, A. and Fruitwala, H. "Correlation of material and processing time scales with structure development in isotactic polypropylene crystallization," Macromol **36**, 6453-6361 (2003).

Ferry, J. D. *Viscoelastic properties of polymers* (Wiley-Interscience, New York, 1980).

Haas, T. W. and Maxwell, B. "Effects of shear stress on crystallization of linear polyethylene and polybutene-1," Polymer Engineering and Science **9**, 225-& (1969).

Hadinata, C., Boos, D., Gabriel, C., Wassner, E., Rullmann, M., Kao, N. and Laun, M. "Elongation-induced crystallization of a high molecular weight isotactic polybutene-1 melt compared to shear-induced crystallization," Journal of Rheology **51**, 195-215 (2007).

Hassager, O., Kolte, M. I. and Renardy, M. "Failure and nonfailure of fluid filaments in extension," J. Non-Newtonian Fluid Mech. **76**, 137-151 (1998).

Huong, D. M., Drechsler, M., Moller, M. and Cantow, H. J. "Electron spectroscopic imaging of polyethylene shish kebabs in situ," Journal of Microscopy **166**, 317-328 (1992).

Janeschitz-Kriegl, H. "How to understand nucleation in crystallizing polymer melts under real processing conditions," Colloid and Polymer Science **281**, 1157-1171 (2003).

Janeschitz-Kriegl, H., Covas, J. A., Agassant, J. F., Diogo, A. C., Vlachopoulos, J. and Walters, K. "Polymer crystallization under process conditions" *Rheological fundamentals of polymer processing* (Kluwer Academic Publishers, 1995)

Keller, A. and Kolnaar, H. W. H. *Flow-induced orientation and structure formation* (Wiley-VCH, New York, 1997).

Kolte, M. I., Rasmussen, H. K. and Hassager, O. "Transient filament stretching rheometry ii: Numerical simulation," Rheol. Acta **36**, 285-302 (1997).

Kumaraswamy, G., Issaian, A. M. and Kornfield, J. A. "Shear-enhanced crystallization in isotactic polypropylene. 1. Correspondence between in situ rheo-optics and ex situ structure determination," Macromolecules **32**, 7537-7547 (1999).

Kumaraswamy, G., Kornfield, J. A., Yeh, F. J. and Hsiao, B. S. "Shear-enhanced crystallization in isotactic polypropylene. 3. Evidence for a kinetic pathway to nucleation," Macromolecules **35**, 1762-1769 (2002).

Larson, R. G. *The structure and rheology of complex fluids* (Oxford University Press, New York, 1999).

Liedauer, S., Eder, G. and Janeschitz-Kriegl, H. "On the limitations of shear-induced crystallization in polypropylene melts," International Polymer Processing **10**, 243-250 (1995).

Lyngaae-Jsrgensen, J. and Sondergaard, K. "Theories of small-angle light, x-ray, and neutron scattering" *Rheo-physics of multiphase polymeric systems* (TECHNOMIC Publishing Co., Lancaster, PA, 1995)

Mackley, M. R. "Shish-kebabs - hydrodynamic factors affecting their crystal-growth," Colloid and Polymer Science **253**, 373-379 (1975).

Mackley, M. R., Frank, F. C. and Keller, A. "Flow-induced crystallization of polyethylene melts," Journal of Materials Science **10**, 1501-1509 (1975).

Mackley, M. R. and Keller, A. "Flow induced crystallization of polyethylene melts," Polymer **14**, 16-20 (1973).

Mackley, M. R. and Keller, A. "Flow induced polymer-chain extension and its relation to fibrous crystallization," Philosophical Transactions of the Royal Society of London Series a-Mathematical Physical and Engineering Sciences **278**, 29-& (1975).

McKinley, G. H. and Sridhar, T. "Filament-stretching rheometry of complex fluids," Annual Review of Fluid Mechanics **34**, 375-415 (2002a).

McKinley, G. H. and Sridhar, T. "Filament stretching rheometry," Annu. Rev. Fluid Mech. **34**, 375-415 (2002b).

Pennings, A. J., Smook, J., Boer, J. D., Gogolewski, S. and Hutten, P. F. V. "Process of preparation of ultra-high strength polyethylene fibers," Pure Appl. Chem. **55**, 777 (1983).

Quirk, R. P. and Alsamarraie, M. A. A. "Physical constants of poly(propylene)". In: Brandup, J. and Immergut, E. H. (Eds.) *Polymer handbook* (Wiley, New York, 1989)

Rothstein, J. P. "Transient extensional rheology of wormlike micelle solutions," J. Rheol. **47**, 1227-1247 (2003).

Rothstein, J. P. and McKinley, G. H. "A comparison of the stress and birefringence growth of dilute, semi-dilute and concentrated polymer solutions in uniaxial extensional flows," J. Non-Newtonian Fluid Mech. **108**, 275-290 (2002a).

Rothstein, J. P. and McKinley, G. H. "Inhomogeneous transient uniaxial extensional rheometry," J. Rheol. **46**, 1419-1443 (2002b).

Samon, J. M., Schultz, J. M., Hsiao, B. S., Seifert, S., Stribeck, N., Gurke, I., Collins, G. and Saw, C. "Structure development during the melt spinning of polyethylene and poly(vinylidene fluoride) fibers by in situ synchrotron small- and wide-angle x-ray scattering techniques," Macromolecules **32**, 8121-8132 (1999).

Schulz, G. "Reptation of entangled polymers," (2001). http://www.fz-juelich.de/iff/G_Schuetz_reptation/. January 11, 2011.

Sentmanat, M., Delgadillo-Velazquez, O. and Hatzikiriakos, S. G. "Crystallization of an ehtylene-based butene plastomer: The effect of unixatial extension," Rheol. Acta **49**, 931-939 (2010).

Shreya, P., S. Verenich, and B. Pourdeyhimi "Blending polypropylene with glycidyl methacrylate-containing polymer to improve adhesion to elastomers," Polymer international **57**, 975-81 (2008).

Tabatabaei, S. H., Carreau, P. J. and Ajji, A. "Rheological and thermal properties of bleands of a long-chain branched polypropylene and different linear polypropylenes," Chemical Engineering Science **64**, 4719-4731 (2009).

Tirtaatmadja, V. and Sridhar, T. "A filament stretching device for measurement of extensional viscosity," J. Rheol. **37**, 1133-1160 (1993).

Van Puyvelde, P., Langouche, F. and Baert, J. "Flow-induced crystallization in poly-1-butene: The shish-kebab transition," International journal of material forming **1**, 667-670 (2008).

Wiesner, U. "Analysis of complex fluids: Small angle x-ray scattering (saxs)," (2008). http://people.ccmr.cornell.edu/~uli/pages/saxs.htm. Jan. 7, 2011.

Yu, F. Y., Zhang, H. B., Liao, R. G., Zheng, H., Yu, W. and Zhou, C. X. "Flow induced crystallization of long chain branched polypropylenes under weak shear flow," European Polymer Journal **45**, 2110-2118 (2009).